

Underestimated Kuroshio power and its potential sites off Southeast Taiwan

Yu-Chia Chang^a, Chau-Ron Wu^{a,b,*}, Peter C. Chu^c, You-Lin Wang^a, Luca R. Centurioni^d, Guan-Yu Chen^e, Ruo-Shan Tseng^e

^a Research Center for Environmental Changes, Academia Sinica, Taiwan

^b Department of Earth Sciences, National Taiwan Normal University, Taiwan

^c Department of Oceanography, Naval Postgraduate School, USA

^d Scripps Institution of Oceanography, University of California San Diego, USA

^e Department of Oceanography, National Sun Yat-sen University, Taiwan

HIGHLIGHTS

- Taiwan's Kuroshio current is an ideal site for ocean current power generation, offering substantial untapped energy potential.
- Measurements show near-surface speeds 25–35 % above models, implying ~70 % underestimation of the power resource.
- Advancing observations and higher-resolution models is vital to harness ocean currents sustainably.
- The study links current speed to capacity factor, enabling energy output and LCOE estimates for commercial viability.

ARTICLE INFO

Keywords:

ocean current energy
optimal siting
ocean current speed
Kuroshio

ABSTRACT

The shift towards a carbon-neutral sustainable society necessitates significant advances in clean and renewable energy worldwide. Ocean currents, characterized by substantial and stable kinetic energy, play a crucial role in accelerating the adoption of this goal. However, there is limited research addressing the optimization of site selection for ocean current power generation. This study makes three key contributions. First, it highlights the optimization of site selection for power generation, with the Kuroshio off the southeastern coast of Taiwan emerging as a highly promising area with substantial potential for harnessing ocean current energy. Second, NOAA drifters, shipboard ADCP transects, and a bottom-mounted mooring each register near-surface speeds 25–35 % higher than co-located HYCOM+NCODA model simulations, indicating that the model underestimates the Kuroshio power resource southeast of Taiwan by approximately 70 %. This finding underscores the importance of continued efforts to improve observational techniques and model resolution, as a comprehensive understanding is critical for effectively utilizing ocean currents as a sustainable energy source. Finally, the study quantifies a strong empirical relationship between flow velocity and turbine capacity factor, enabling initial estimates of energy output and levelized cost of energy (LCOE) for the preferred site.

1. Introduction

The United Nations 2030 Agenda was launched in 2015, setting forth the Sustainable Development Goals (SDGs) for a collectively prosperous and sustainable world [1]. Among these goals, climate change is addressed through the utilization of sustainable and renewable energy sources [2,3]. Global ocean currents are an alternative source of clean energy due to their persistence and sustainability [4–6]. Western boundary currents, such as the Kuroshio and Gulf Stream, are characterized by steep lateral pressure gradients and narrow jet widths. The

Kuroshio Current is a powerful, warm, and saline western boundary current that flows northward along the western edge of the North Pacific Ocean. It features high velocity and substantial volume transport, originating near the Philippines and passing east of Taiwan and south of Japan (Fig. 1a). Such western boundary currents are therefore ideally suited for ocean current power generation. For example, the overall kinetic energy flux of the Gulf Stream is equivalent to 20–25 GW [7–9]. The power density of the Gulf Stream near the North Carolina (Florida) shore is estimated to be approximately 500–1000 (3000) W/m² [10]. Exploiting the Kuroshio east of Taiwan has the potential to generate

* Corresponding author at: Research Center for Environmental Changes, Academia Sinica, Taiwan

E-mail address: cwu@ntnu.edu.tw (C.-R. Wu).

<https://doi.org/10.1016/j.apenergy.2025.126316>

Received 27 March 2025; Received in revised form 10 May 2025; Accepted 9 June 2025

Available online 12 June 2025

0306-2619/© 2025 The Authors. Published by Elsevier Ltd. This is an open access article under the CC BY-NC-ND license (<http://creativecommons.org/licenses/by-nc-nd/4.0/>).

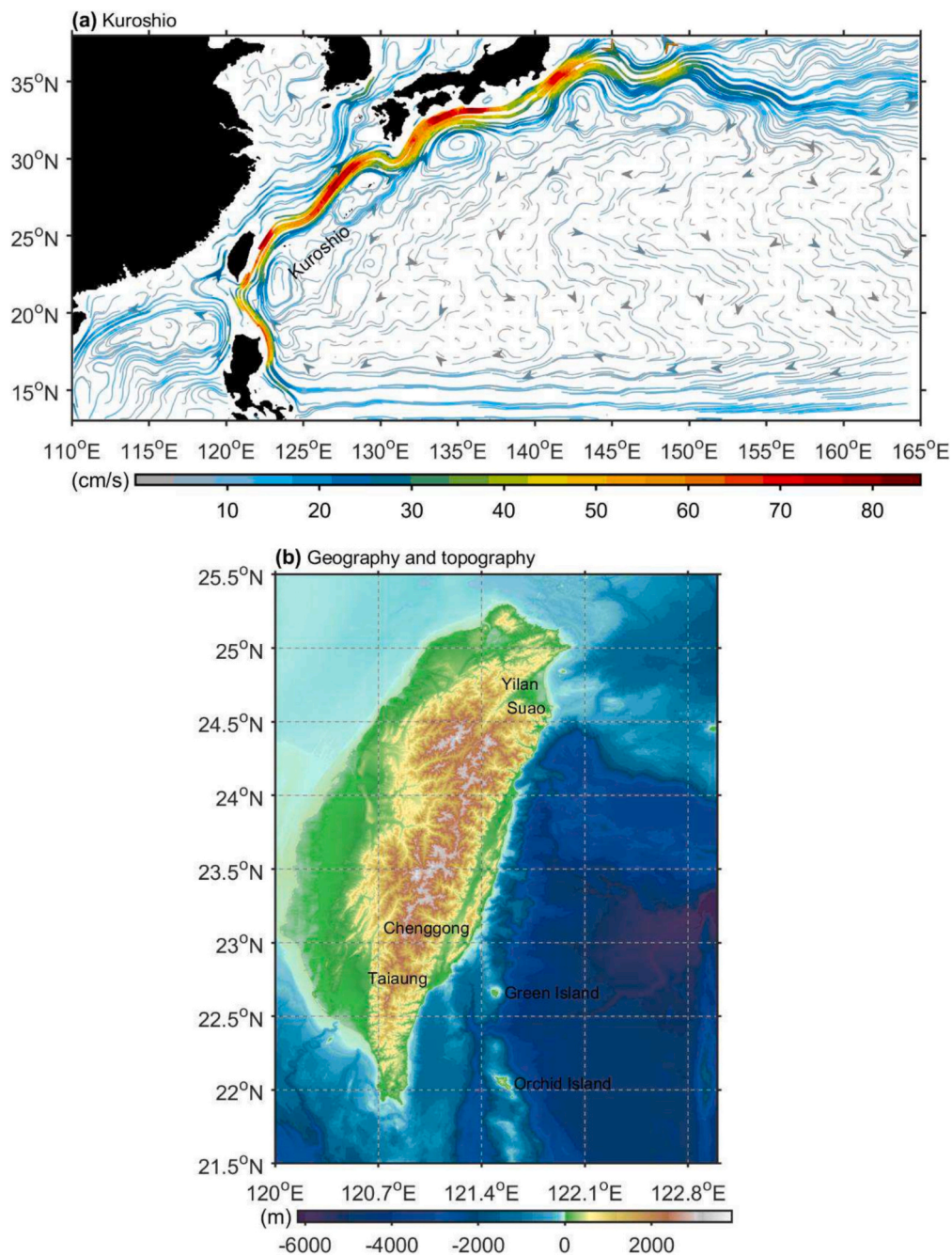


Fig. 1. (a) Climatological-mean geostrophic velocity field of the Kuroshio Current (1993–2022) derived from satellite altimetry, with colour shading representing flow magnitude. (b) Geography and bottom topography of the Kuroshio power plant. Bathymetric, topographic, and shoreline data are obtained from the NOAA National Centers for Environmental Information.

24–30 GW of kinetic energy flux based on numerical model data [11,12]. The Kuroshio off the eastern coast of Taiwan can provide annual electricity of approximately 92TWh [13], which accounts for approximately 33 % of Taiwan’s annual electricity consumption in 2022. However, the siting of current-based power plants often relies on numerical model simulations, which are prone to significant uncertainties [11,12,14]. For example, incorrect selection of the model grid size leads to an inaccurate bottom topography. Barnier et al. [14] used grid sizes of $1/12^\circ$ (ORCA12) and $1/36^\circ$ (ORCA36) to estimate the theoretical available power (TAP). The TAP of ocean currents was ~ 450 MW and ~ 810 MW; thus, the higher the resolution, the higher the TAP. Additionally, HYCOM data has been shown to underestimate ocean current energy densities off the coasts of South Africa and Florida (USA)

when compared with Acoustic Doppler Current Profiler measurements [15]. It is important to note that validation is most meaningful when applied to a specific numerical model and is limited to the particular location where the validation was conducted.

In Japan, significant progress has been achieved in ocean current power generation technology. In 2016, an ocean current turbine with a 2-m rotor diameter and a rated power of 1 kW successfully generated approximately 260 W at a towing speed of 1 m/s [16]. Building on this foundation, the 100-kW-class “Kairyu” turbine was developed through a collaboration between IHI Corporation and the New Energy and Industrial Technology Development Organization (NEDO). This turbine features an 11-m rotor diameter and two 50 kW units [16]. In 2017, the Kairyu turbine demonstrated its capabilities by generating

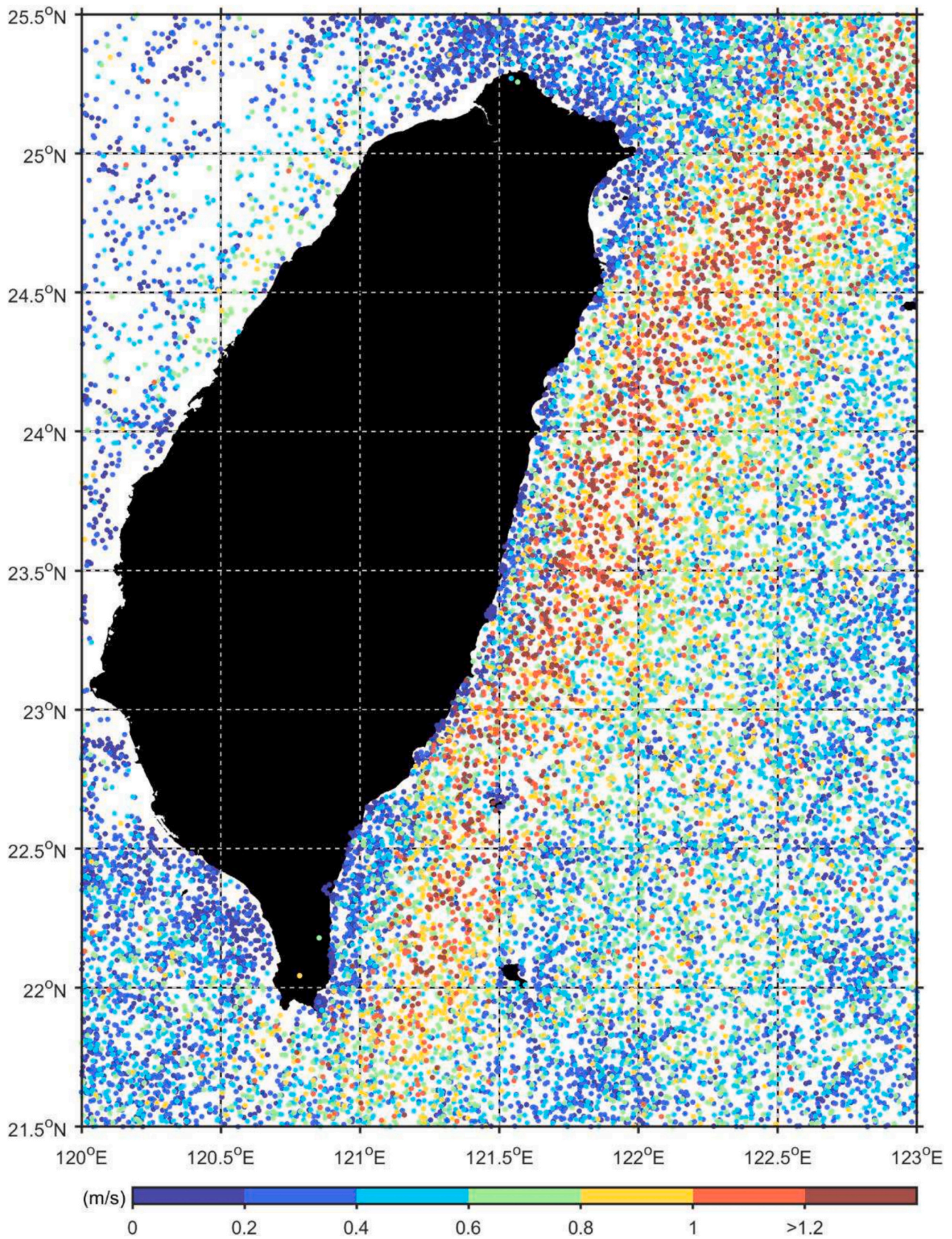


Fig. 2. The surface velocity (15 m depth) derived from drifter observations. The dots represent the tracks of the drifters, while its colour corresponds to velocities.

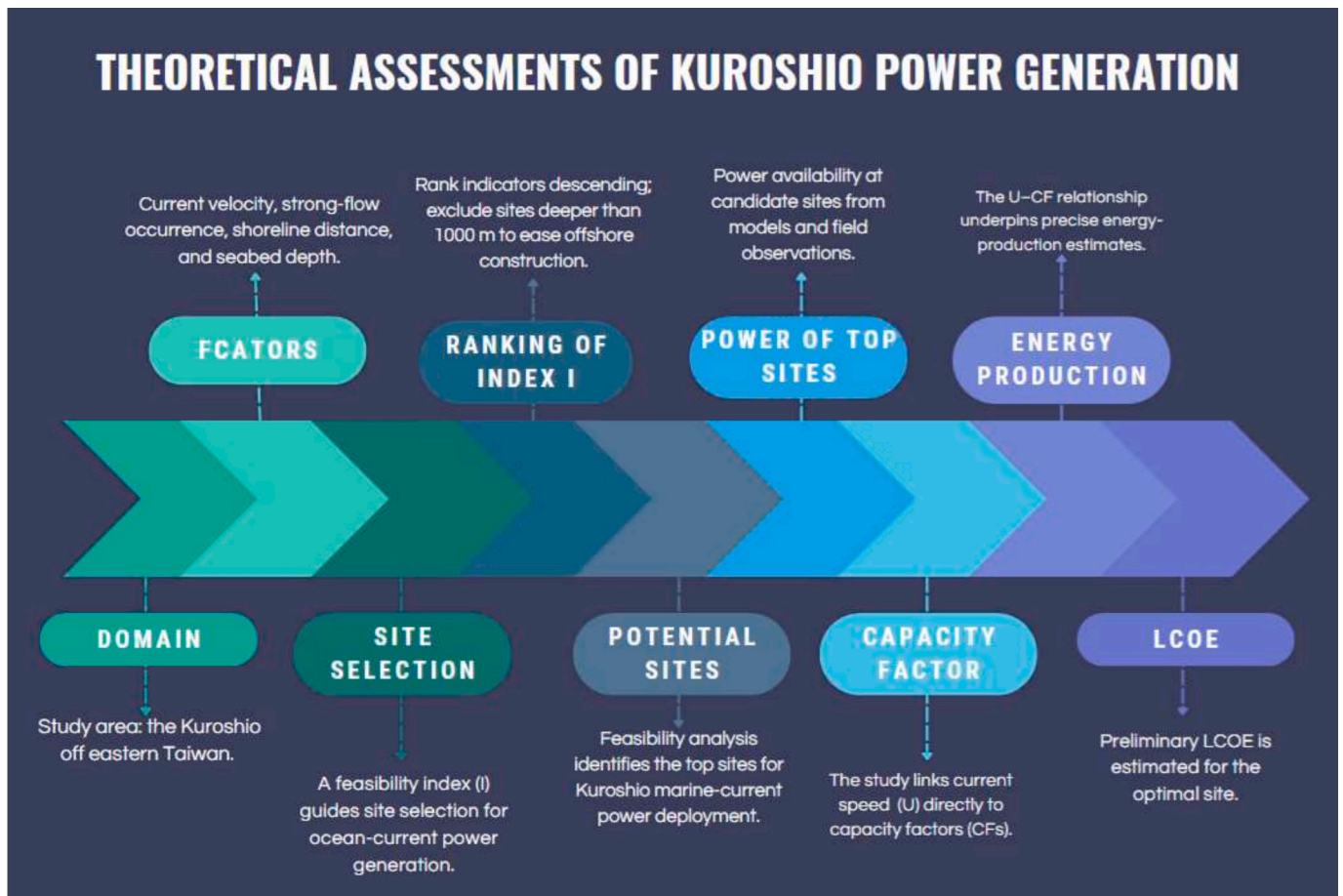


Fig. 3. Methodological workflow for theoretical assessments of Kuroshio-current power generation off eastern Taiwan. The schematic summarizes the sequential analyses used in this study. Domain definition: the investigation is confined to the western boundary current east of Taiwan. Site-selection screening: four geophysical indicators—mean current velocity (U), percentage occurrence of strong flow (P), distance to shoreline (L), and seabed depth (D)—are ranked to construct a composite feasibility index I , with sites deeper than 1000 m excluded. Identification of potential sites: the highest-ranking grid cells constitute candidate locations for turbine deployment. Capacity-factor evaluation: observational and model data are used to derive site-specific capacity factors (CFs) via the empirical U -CF relationship. Energy and cost appraisal: annual energy production and a preliminary leveled cost of energy (LCOE) are calculated for the optimum site(s).

approximately 30 kW of power at a current speed of 1.0 m/s in the Kuroshio near the Tokara Islands, reaching its rated power output of 100 kW at a towing speed of 1.5 m/s [17]. Efforts are currently underway to advance this technology further, with the development of a 2 MW turbine featuring a 40-m rotor diameter [17].

Taiwan has also made significant strides in marine energy systems. In 2015, Wan Chi Steel (WCS) Industrial Co. introduced a 50-kW current turbine capable of generating approximately 33 kW of power at a current speed of nearly 1.4 m/s [18–20]. In 2016, a deep-sea mooring system and a floating platform were successfully installed in the Kuroshio's mainstream at a depth of 900 m [18–20]. The 50-kW turbine deployed in the Kuroshio's mainstream generated an average of 26 kW of power at a current speed of approximately 1.3 m/s and demonstrated continuous operation for 60 h, even at low current speeds of 0.45 m/s [18–20]. Further advancements came in 2020, when Taiwan tested a 0.2 MW deep-water current turbine developed by WCS, marking another milestone in the development of marine energy technology.

Despite these advancements, existing studies have not yet established the relationship between capacity factors of ocean current turbines and current speeds, which is crucial for accurate energy production estimation and leveled cost of energy assessment. Furthermore, the identification of suitable sites for ocean current power plants in Taiwan remains unclear. This study seeks to address the following key scientific questions: (i) Has the power generation capacity of ocean currents, such as the Kuroshio, been significantly

underestimated when relying on model data? (ii) What is the relationship between ocean current speeds and capacity factors? (iii) Where are the most suitable locations for Kuroshio power plants to harness sustainable energy?

To address these questions, we integrate multiple data sources: NOAA Global Drifter trajectories, HYCOM+NCODA 1/12° analysis-reanalysis fields, CMEMS altimeter-derived surface velocities, and high-resolution Eulerian currents from moored and shipboard ADCP measurements. The present paper is structured as follows. Section 2 covers the methodology. Section 3 discusses the suitable sites for Kuroshio power generation, capacity factors of ocean current energy, and the underestimated potential of Kuroshio power, with detailed analysis of these results. Finally, Section 4 presents the conclusion.

2. Methodology

2.1. Data

This study synthesizes five complementary data streams: (i) NOAA Global Drifter Program trajectories (1989–2012) [21]; (ii) shipboard ADCP sections collected from 1991 to 2017 [22]; (iii) CMEMS altimeter-derived currents spanning 1993–2023 [23]; (iv) HYCOM+NCODA global 1/12° analysis-reanalysis fields for 1995–2022 [24]; and (v) a project-specific moored-ADCP time series. The GDP drifters had a holey-sock drogue centered at a nominal depth of 15 m and were deployed in

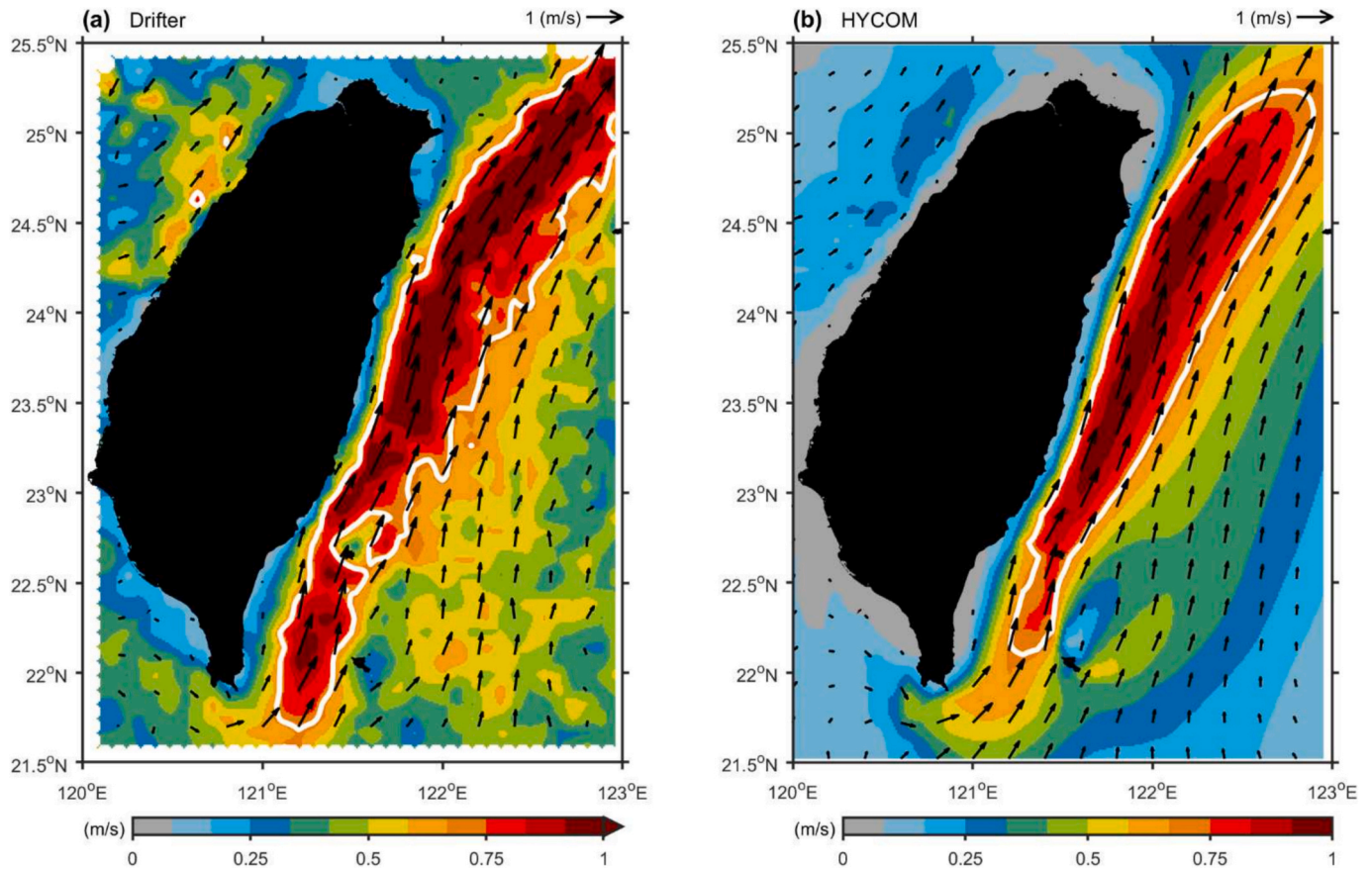


Fig. 4. Temporally averaged current speeds and vectors from (a) drifter data and (b) the HYCOM+NCODA 1/12° reanalysis data at 15 m depth.

or drifted into the Kuroshio current at the study area (21.5°–25.5°N, 120°–123°E) (Fig. 1b). The GDP drifters obtained 22,103 6-hourly velocity observations in the study area (Fig. 2). The Drifter Data Assembly Center at NOAA's AOML provides quality-controlled data for velocity measurements. The estimated accuracy of the velocity measurements using GDP drifters is ~ 0.01 m/s with surface winds of 10 m/s [25]. GDP drifter data can be obtained from the website [26]. Shipboard ADCP velocities were acquired aboard the four Taiwanese research vessels. Satellite data were obtained from the CMEMS multi-mission altimetry product, in which sea level anomalies are optimally interpolated from along-track observations of successive altimeter missions and expressed relative to a 1993–2012 mean sea surface. The product also supplies absolute dynamic topography and the corresponding geostrophic current fields. The HYbrid Coordinate Ocean Model (HYCOM) is an open-source, ocean general circulation modeling system that combines three coordinate systems: the isopycnal coordinate in the open ocean, the terrain-following coordinate in shallow regions, and the z-level coordinate in the mixed layer. HYCOM uses the Navy Coupled Ocean Data Assimilation (NCODA) system to assimilate available satellite observations as well as in-situ vertical temperature and salinity profiles [27,28]. In 2023 we deployed a bottom-mounted mooring in the Kuroshio off southeastern Taiwan. The instrumentation package comprised an upward-looking ADCP, syntactic-foam flotation, a galvanized-steel tether, an acoustic-release unit, and an anchor block.

2.2. Methods

The workflow in Fig. 3 presents the methodological framework employed to assess the theoretical power potential of the Kuroshio Current east of Taiwan. The western boundary jet adjacent to Taiwan was first delineated as the study domain. Four geophysical indicators

(ocean current velocity, frequency of strong flow occurrences, distance from the shoreline, and water column depth) were normalized and combined into a single, dimensionless feasibility index [13,29,30]. Grid cells exceeding 1000 m in depth were excluded a priori to reflect engineering limitations. The highest-ranked cells by index value were then grouped into provisional turbine corridors. Within these priority corridors, preliminary estimates of annual energy yield and leveled cost of energy (LCOE) were computed based on the empirically derived relationship between current speed and capacity factor.

A formal definition of the composite feasibility index used to rank candidate sites is presented below. Key siting criteria for marine current power installations comprise proximity to the coastline, limited water depth, and high, temporally stable flow velocities [13,29,30]. Near-shore, shallow-water locations reduce foundation and cable costs and simplify maintenance logistics, while persistently strong currents ensure dependable energy yields and, consequently, attractive project economics. In 2015, a feasibility index (I) was proposed to determine site selection for current power generation, as shown in Eq. (1) [29,30],

$$I = \sum_{i=1}^4 I_i w_i \quad (1)$$

$$I_1 = \left[1 - \left(\frac{L}{50\text{km}} \right) \right], I_2 = \left[1 + \left(\frac{D}{1000\text{m}} \right) \right], I_3 = P(U > 0.7 \text{ m/s}), I_4 = \frac{U}{1.4 \text{ m/s}}$$

where L is the distance from shore, D and U are the depth and current speed at that site, and P is the percentage of current speed > 0.7 m/s. At a towing speed of 0.7 m/s, the 1 kW current turbine can start to generate an electrical output of approximately 80 W in the previous experiment [16]. Other constants (50 km, -1000 m, 1.4 m/s) were chosen to follow

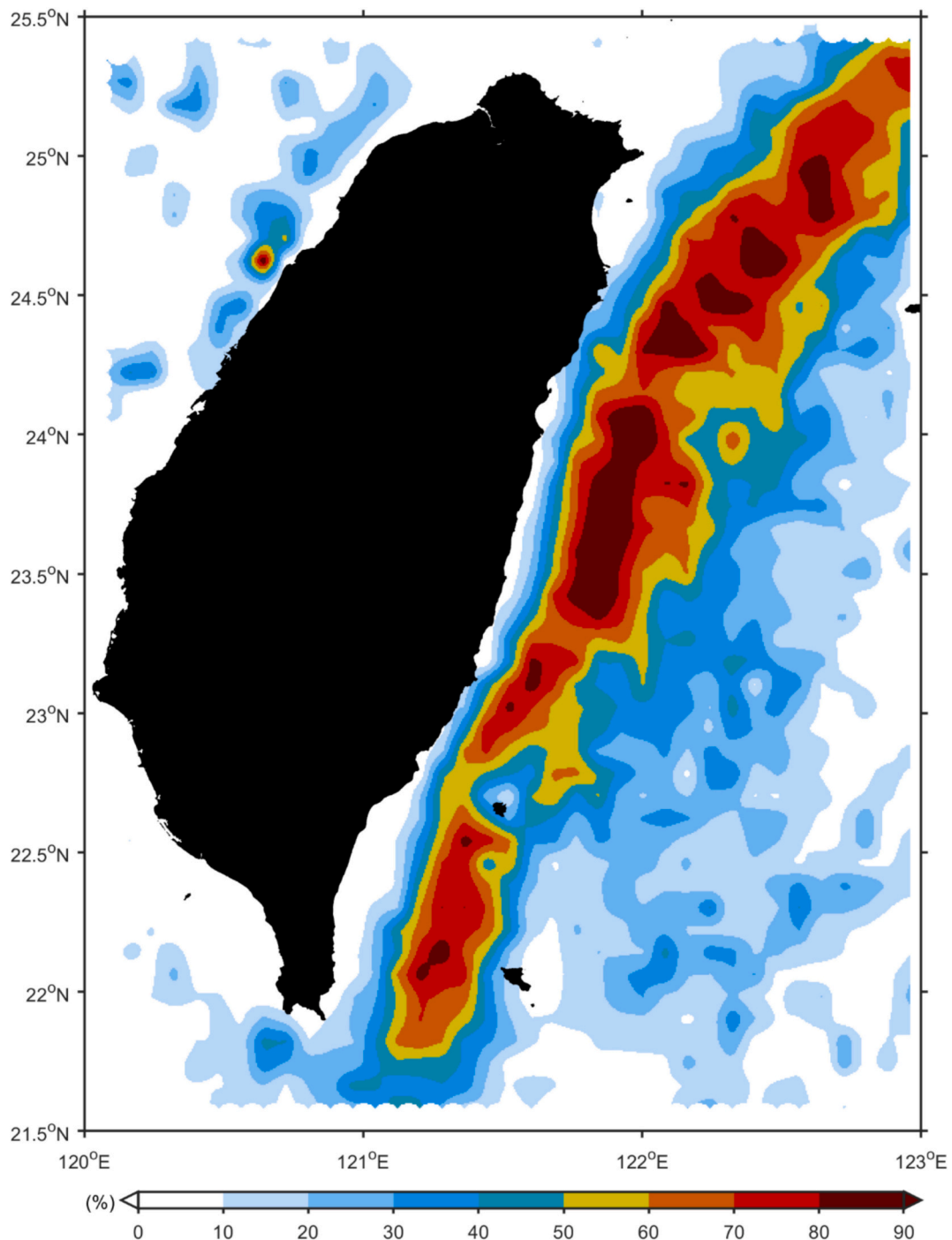


Fig. 5. Percentages of current speed >0.7 m/s.

the typical values of previous studies [13,29,30] for site selection of ocean current power generation. Smaller L and D values reduce a power plant's engineering and maintenance costs. On the other hand, larger P and U values increase the revenue of the power plant. If the plant's life is 20 years, expenses and revenue are $\sim 31\%$ (146 million USD) and $\sim 69\%$ (319 million USD), respectively [13,29,30]. In Eq. (1), each value of (I_i) was weighted (w_i) to reflect its impact on capital costs, maintenance costs ($w_1=15.5\%$; $w_2=15.5\%$), and revenue ($w_3=34.5\%$; $w_4=34.5\%$) [29,30].

The feasibility index (I) for site selection in ocean current power generation integrates key factors influencing the costs and revenues of potential power plants. Each component of the index is meticulously

chosen to ensure a comprehensive evaluation of site suitability. By balancing these critical factors, the feasibility index provides a robust and holistic measure for identifying optimal locations for current power generation. The index incorporates parameters such as distance, depth, current speed, and the percentage of high-speed currents. This approach ensures that selected sites maximize power generation potential while minimizing costs, facilitating the development of economically viable and sustainable ocean current power plants.

In this study, site-specific capacity factors (CFs) are obtained from an empirical U -CF relationship constrained by existing data. The electricity production and $LCOE$ are calculated for the optimal sites, linking physical resource quality to techno-economic performance. The $LCOE$ is

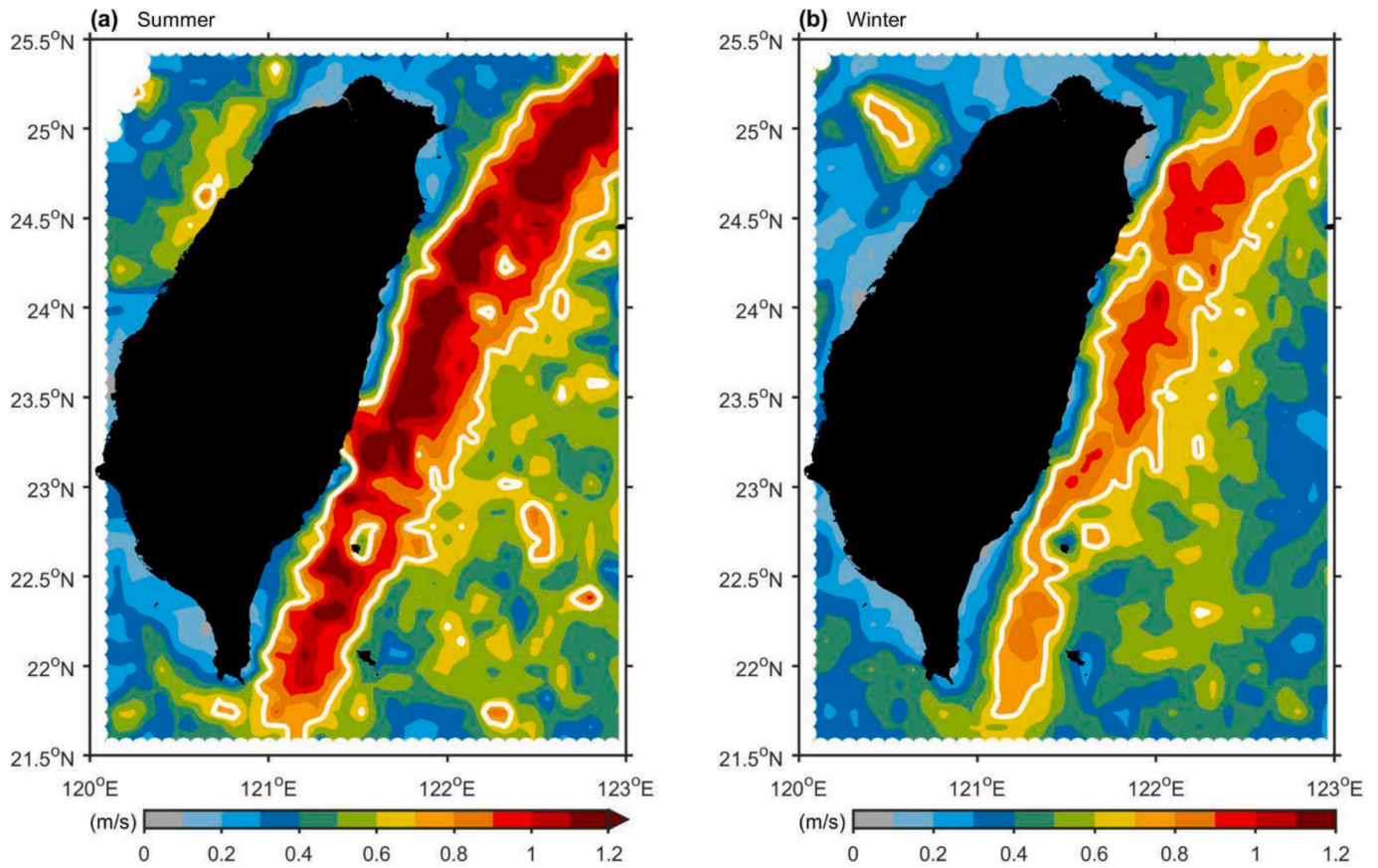


Fig. 6. Typical drifter speeds (unit: m/s) (a) in summer (April–September) and (b) winter (October–March) half-years.

calculated by dividing the lifetime costs (LC_s) by the energy productions (EP_s),

$$LCOE = \frac{LC_s}{EP_s} = \frac{\sum_{t=1}^n \frac{ICC_t + AOE_t}{(1+DR)^t}}{\sum_{t=1}^n \frac{EP_t}{(1+DR)^t}} \quad (2)$$

where the subscript t denotes the year, ICC_t is the initial capital cost, AOE_t represents the annual operating expenses, AFE_t denotes the annual fuel expenses, EP_t is the annual energy production, DR is the discount rate, and n is the system's lifetime in years. This end-to-end framework couples physical oceanography with cost metrics, offering a transparent template for marine current resource assessments in other western boundary current regimes.

3. Results and discussion

3.1. Kuroshio power generation and suitable sites

Fig. 1b shows the bottom topography (i.e., ETOPO1 data) obtained from NOAA's National Centers for Environmental Information (NCEI). Coastline data from NCEI can be used to calculate the distance from shore. The ensemble of the individual drifter observations is plotted in Fig. 2, colour coded in accordance with the local instantaneous speed. The ensemble mean current speed (Fig. 4) and velocity vectors (Fig. 5) at 15 m depth, determined from observed drifter data, were computed using the bin average method [31–36] in $1/12^\circ \times 1/12^\circ$ bins, comparable to the grid size of the HYCOM+NCODA $1/12^\circ$ reanalysis data. A complete map of the strong Kuroshio currents east of Taiwan, generated from direct velocity measurements collected over 24 years (1989–2012), is shown in Fig. 4a. Mean current speeds and vectors at 15 m depth, as determined from the HYCOM+NCODA data of 1995–2012, are shown in Fig. 4b. Green Island ($22^\circ 39' 26.5''N$ $121^\circ 28' 32.6''E$), with an area of

$\sim 16 \text{ km}^2$, is treated as ocean in the HYCOM+NCODA $1/12^\circ$ model ($1/12^\circ \times 1/12^\circ$ is $\sim 73 \text{ km}^2$ at $\sim 22.6^\circ N$). The temporally averaged speeds reached a maximum of nearly 1.1 m/s east of Taiwan according to the GDP drifter data (Fig. 4) and of $\sim 0.9 \text{ m/s}$ according to the HYCOM+NCODA data. The current speed according to the HYCOM+NCODA model was thus $\sim 20 \%$ lower than the observed drifter speed. The percentages of current speed $> 0.7 \text{ m/s}$ (i.e., the percentage of a good quality power supply) in $1/12^\circ \times 1/12^\circ$ bins reached 80–90% (~ 19.2 – 21.6 h/day) in the mainstream of the Kuroshio (Fig. 5). The seasonal variations in Kuroshio current speeds are reported as averaged drifter speeds in Fig. 6 for the summer (April to September) and winter (October to March) half-years. The mean Kuroshio speeds were higher in summer (1.2–1.3 m/s) than in winter (0.9–1.0 m/s) half-years, by 0.2–0.3 m/s. Therefore, the Kuroshio power plant will generate more electricity and meet Taiwan's high demand for electricity in summer.

Fig. 7 shows the distribution of the feasibility index (I) in the Kuroshio region. Priority sites for developing Kuroshio current power generation are present at Chenggong, Green Island, and Yilan. The information and location of the six suitable sites for current power generation are listed in Table 1, based on the mean drifter velocities in Fig. 4 and the isobaths in Fig. 8. Among these sites, five (C1–C5) are located east of Chenggong and one site (G1) is situated southwest of Green Island (Fig. 8). The I values ranged from 0.54 to 0.68 for C1–C5 and 0.51 for G1, with a maximum of 0.68 at C1 (Table 1). This suggests that the C1 site ($121.44^\circ E$, $22.94^\circ N$, $1/12^\circ \times 1/12^\circ \sim 73 \text{ km}^2$), located southeast of Chenggong, is the most suitable for the development of Kuroshio current power generation, given its stability ($P = 77 \%$), high current speed ($U = 1.1 \text{ m/s}$), acceptable distance to the coast ($L = 22 \text{ km}$), and water depth ($D = 580 \text{ m}$).

Sensitivity refers to the degree to which the characteristics of the system are affected by parameter variation. The results of the sensitivity

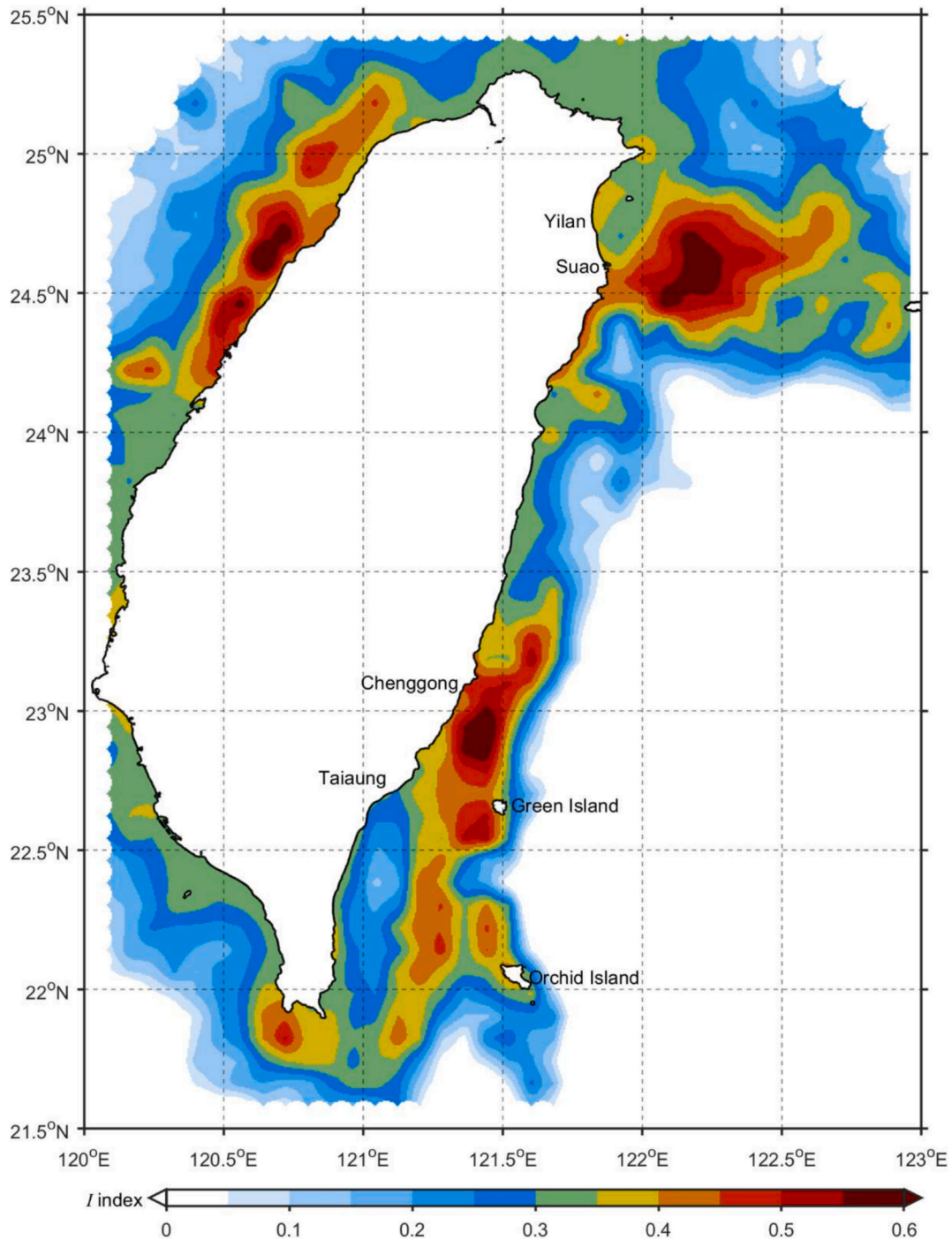


Fig. 7. Distribution of the feasibility index (*I*) in the Kuroshio region.

Table 1
Six suitable locations for development of Kuroshio current power generation.

No.	Site	Place-name	Location	the feasibility index (<i>I</i>)
1	C1	Chenggong	121.44°E, 22.94°N	0.68
2	C2	Chenggong	121.44°E, 22.86°N	0.62
3	C3	Chenggong	121.36°E, 22.86°N	0.58
4	C4	Chenggong	121.36°E, 22.94°N	0.55
5	C5	Chenggong	121.44°E, 23.02°N	0.54
6	G1	Green Island	121.44°E, 22.62°N	0.51

analysis are shown in Fig. 9. The areas selected based on their high feasibility index (*I*) values were not changed significantly in response to parameter variations. Table 2 lists the location, distance, depth, percentage, and speed of the five most suitable sites (C1–C5 sites in Fig. 8) for the development of Kuroshio current power generation. At 22.9°N (see Fig. 8), the distance corresponding to 1/12° is approximately 8.53 km. At the native 1/12° resolution a single HYCOM grid cell (~8 km × 8 km, ~73 km²) covers an area an order of magnitude larger than that required for turbine micro-siting; the five highest-scoring cells (C1–C5) therefore span approximately 365 km² in aggregate. While this coarse, theory-driven filter efficiently highlights broad corridors of interest, its spatial granularity imposes substantive constraints that must be

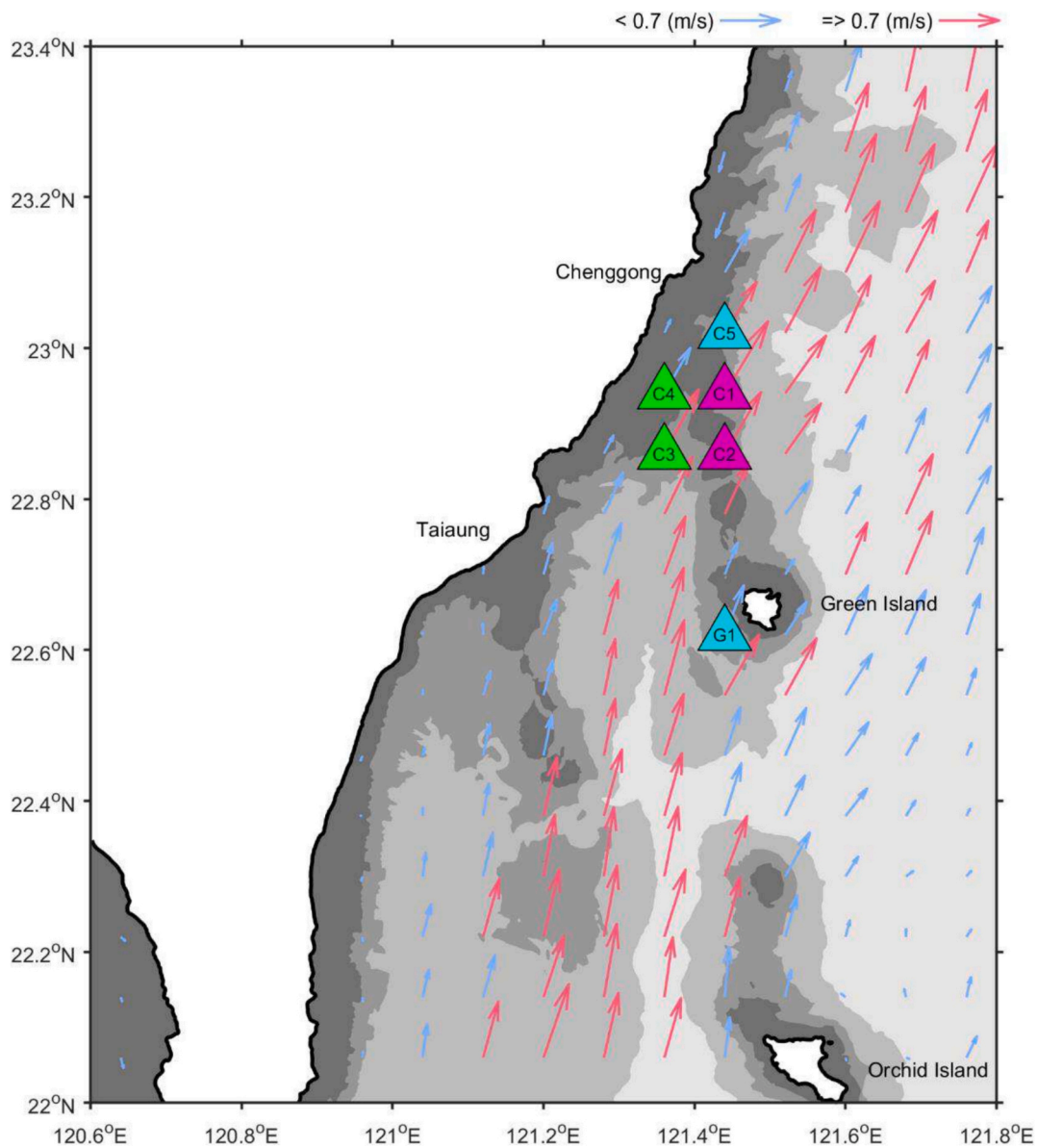


Fig. 8. Typical drifter speeds as well as the 6 suitable sites located east of Chenggong (C1–C5 sites) and southwest of Green Island (G1 site). The contours represent the isobaths (–500 m, –1000 m, and –2000 m). Red (blue) arrows indicate a current speed greater (less) than 0.7 m/s. (For interpretation of the references to colour in this figure legend, the reader is referred to the web version of this article.)

explicitly acknowledged. Barnier et al. [14] assumed that a conceptual power plant has 315 turbines (or 630 rotors) over an area of 100 km². These 315 turbines would collectively occupy approximately 1.8 km², representing only 1.8 % of the total area. Consequently, they considered it reasonable to assume that the interaction between the turbines would be negligible.

Thus, 1150 turbines ($315 \times 365 \div 100 \cong 1150$) can be deployed across the area covered by the C1–C5 sites (~ 365 km²) (Fig. 8). With Japan's plan to develop turbines featuring a rated output of 2 MW and a rotor diameter of approximately 40 m, these 1150 turbines could collectively achieve a rated output of 2.3 GW. However, it is crucial to consider turbine efficiency when planning the installation of such large arrays. The rated output does not account for the efficiency of energy extraction, meaning the actual power generation would depend on the turbines' effectiveness in converting kinetic energy from ocean currents into electrical energy. This highlights the need for detailed efficiency evaluations to ensure accurate projections and the successful implementation of ocean current power projects.

3.2. The capacity factor and cost of ocean current power generation

The power curve represents the relationship between ocean current speed and the expected power produced. A linear regression equation, Eq. (2), was derived from the towing (or current) speed (U) and the capacity factor (CF) in Japan and Taiwan (Table 3), based on results of previous studies [16–20]:

$$CF = 0.895U - 0.574 \quad (0.5 \text{ m/s} \leq U \leq 1.5 \text{ m/s}) \quad (2)$$

The correlation coefficient for the analysis was notably high ($R = 0.94$), with a root mean square error (RMSE) of 0.303. Fig. 10 illustrates the relationship between current (or towing) speeds and CF s. When the current speed (U) is below 0.5 m/s, CF is assumed to be 0, and when U exceeds 1.5 m/s, CF is considered to be 1. A polynomial equation, $CF = 0.876U^2 - 0.885U + 0.256$, was fitted to the data shown in Fig. 10, resulting in an improved RMSE of 0.276. Typically, CF is defined as the unitless ratio of the power produced over a given period to the rated power during that same period. In this study, CF specifically denotes the

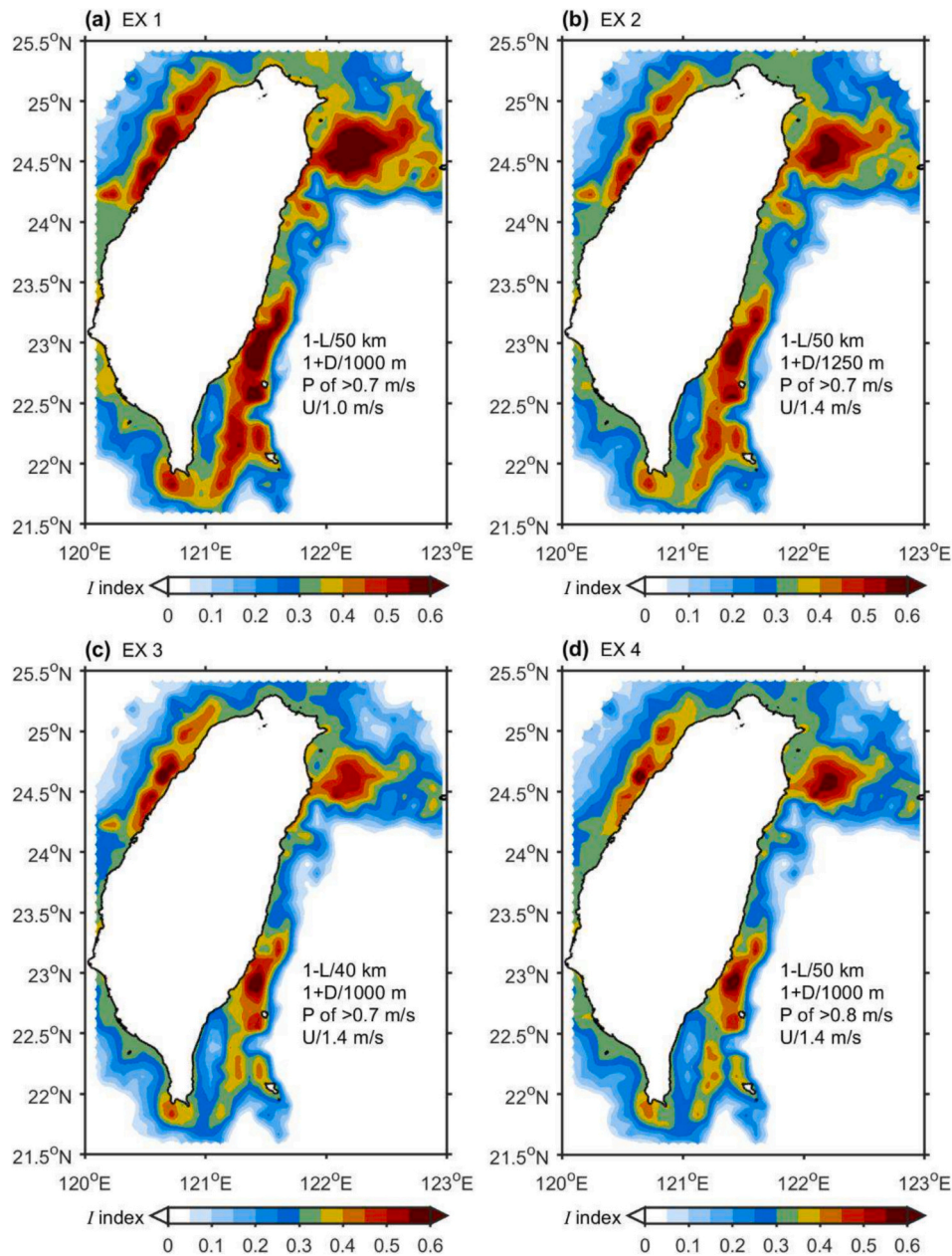


Fig. 9. Sensitivity of the *I* index to parameter variation. (a) 1- *L*/50 km, 1+ *D*/1000 m, $P(U>0.7 \text{ m/s})$, $U/1.0 \text{ m/s}$, (b) 1- *L*/50 km, 1+ *D*/1250 m, $P(U>0.7 \text{ m/s})$, $U/1.4 \text{ m/s}$, (c) 1- *L*/40 km, 1+ *D*/1000 m, $P(U>0.7 \text{ m/s})$, $U/1.4 \text{ m/s}$, and (d) 1- *L*/50 km, 1+ *D*/1000 m, $P(U>0.8 \text{ m/s})$, $U/1.4 \text{ m/s}$.

Table 2

Expenses and revenue factors of the top five suitable locations for development of Kuroshio current power generation. Speeds refer to typical drifter speeds at five suitable locations.

Site	Location	Distance, <i>L</i> (km)	Depth, <i>D</i> (m)	Percentage, <i>P</i> (%)	Speed, <i>U</i> (m/s)
C1	121.44°E, 22.94°N	22	-580	77 %	1.06
C2	121.44°E, 22.86°N	29	-510	72 %	0.91
C3	121.36°E, 22.86°N	20	-710	63 %	0.93
C4	121.36°E, 22.94°N	11	-220	40 %	0.70
C5	121.44°E, 23.02°N	18	-640	58 %	0.76

ratio of produced power to rated power during periods of consistent towing (or current) speeds, providing a more detailed representation of the relationship between speed and power generation efficiency.

For a typical Kuroshio current speed of 1 m/s, the generated power of a rotor is ~30 % of the rated power. If the current speed is increased to 1.4 m/s, the generated power is ~70 % of the rated power. If a large turbine with a rated power of 2 MW can generate ~30 % of the rated power at a typical current speed of 1 m/s, then 1150 turbines over the area of the C1–C5 sites will generate ~690 MW (2300 MW × 30 % = 690 MW) of power. It is important to note that the 690 MW estimate assumes a current speed of 1 m/s for each turbine and does not account for hydrodynamic interactions between turbines. These interactions can influence the overall performance of the turbine array, potentially reducing the efficiency of power generation in real-world conditions.

The capacity factor is a key indicator for the feasibility of a technology at a given location. Capacity factor values above 0.2–0.3 are clear indicators of feasibility. The velocity of the Kuroshio contains

Table 3
Results of towing experiments in Japan and Taiwan for the Kuroshio power generation.

Year	Japan/ Taiwan	Rate power (RP)	Towing (or current) speed	Generated power (GP)	Capacity factor (CF) (CF = GP/RP)
2016	Taiwan	50 kW	0.5 m/s (startup)	0 kW	0.00
2016	Japan	1 kW	0.7 m/s	0.08 kW	0.08
2016	Japan	1 kW	0.8 m/s	0.12 kW	0.12
2016	Japan	1 kW	0.9 m/s	0.19 kW	0.19
2016	Japan	1 kW	1.0 m/s	0.26 kW	0.26
2017	Japan	100 kW	1.0 m/s	30 kW	0.30
2016	Japan	1 kW	1.1 m/s	0.34 kW	0.34
2016	Japan	1 kW	1.2 m/s	0.41 kW	0.41
2016	Taiwan	50 kW	1.3 m/s	26 kW	0.52
2015	Taiwan	50 kW	1.4 m/s	33 kW	0.66
2017	Japan	100 kW	1.5 m/s	100 kW	1.00

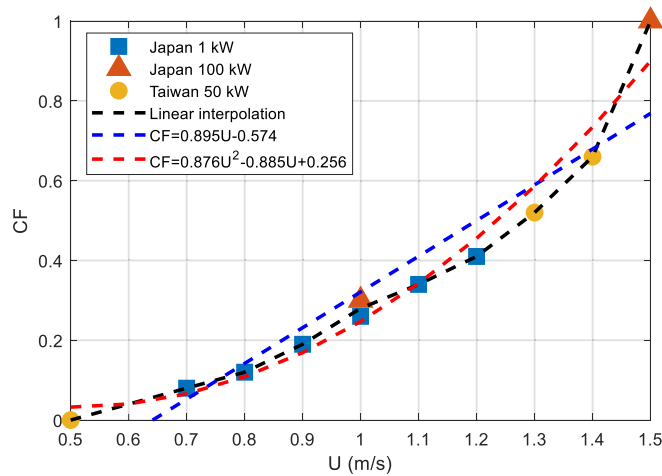


Fig. 10. Relationship between towing (current) speeds and the capacity factor (CF) for ocean current turbines.

seasonal variations [37]. The mean Kuroshio speeds and capacity factors were higher in summer (1.2–1.3 m/s; $CF=0.5\text{--}0.6$) than winter (0.9–1.0 m/s; $CF=0.2\text{--}0.3$), as shown in Figs. 6 and 10. In terms of capacity factor, Kuroshio power generation achieves values of 0.2–0.3 (CF) in both summer and winter. Taiwan Power Company’s electricity sales during summertime and wintertime of 2023 were 120,992 GWh and 112,047 GWh, respectively [38]. 1150 turbines over the area of the C1–C5 sites will generate approximately 5541 GWh ($2300\text{ MW} \times 0.55 \times 365\text{ days}/2 \times 24\text{ h} = 5,540,700\text{ MWh}$) and 2519 GWh ($2300\text{ MW} \times 0.25 \times 365\text{ days}/2 \times 24\text{ h} = 2,518,500\text{ MWh}$) of electricity in summer and winter, respectively. Kuroshio power energy over the area of the C1–C5 sites constitutes 4.6 % and 2.3 % of Taiwan’s total energy demand on summer and winter days of 2023, respectively.

The 30 MW Kuroshio array is projected to deliver 5.541 TWh in summer and 2.519 TWh in winter, totaling 8.06 TWh over its 20-year operational life. Multiplying this output by Taiwan’s 2024 grid-average emission factor ($0.474\text{ kg CO}_2\text{ kWh}^{-1}$) [39] yields the avoided carbon footprint. Preliminary estimates suggest a lifetime reduction of approximately 3.82 million tons of CO_2 . A representative pre-commercial Kuroshio pilot array rated at 30 MW is projected to incur a present-value life-cycle expenditure of US \$146 million, assuming a 20-yr service life and an 8 % discount rate [11,29]. At the best-performing site, depth-averaged near-surface speeds reach 1.2–1.3 m/s in summer and 0.9–1.0 m/s in winter, yielding capacity factors (CFs) of 0.50–0.60 and 0.20–0.30, respectively. These hydrodynamic conditions translate to preliminary LCOE of US \$94–113 MWh^{-1} for the summer

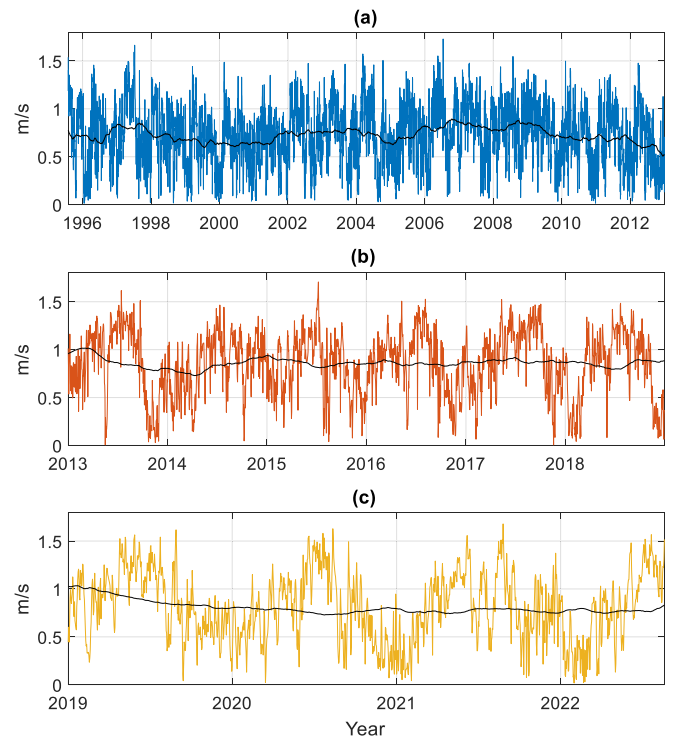


Fig. 11. Time series of 15 m depth current speeds at the C1 site from HYCOM+NCODA $1/12^\circ$ datasets: (a) GLBu0.8 reanalysis (1995–2022; mean = $0.73 \pm 0.31\text{ m/s}$), (b) GLBv0.8 analysis (2017–2022; mean = $0.85 \pm 0.34\text{ m/s}$), and (c) GLBy0.8 analysis (2019–2022; mean = $0.81 \pm 0.36\text{ m/s}$). Black curves denote the 13-month running-mean-filtered records. Over the full 27-year HYCOM period, the Kuroshio’s flow speed off southeastern Taiwan exhibits high interannual stability with no evidence of the large-amplitude meanders characteristic of the southern Japan sector.

half-year and US \$187–283 MWh^{-1} for the winter half-year. Economies of scale are expected to drive the LCOE substantially lower as array size increases; notably, a Minesto techno-economic assessment [40] forecasts an LCOE of US \$54 MWh^{-1} once cumulative installed capacity reaches 100 MW.

Previous studies [11,41] found that turbines with a vertical axis may be suitable for a Kuroshio power plant because the construction and maintenance costs of such turbines are lower than those of other deep-sea engineering projects. However, at present, most generators, including those developed in the USA, Japan, and Taiwan, are based on horizontal axis turbines [14,16,17]. As noted above, $\sim 11\text{ km}$ of submarine cable was successfully installed at an offshore site by the MeyGen project in 2015 [42], and submarine cables installed over longer distances should be feasible in the future. A mooring system for a single generator in deep water was successfully tested by Japan and Taiwan during 2016–2017 [17–20]. The relay platform for multiple generators is a flexible structure that floats in deep waters [43,44] and is tethered via cables and chains to the seabed, allowing considerable freedom of movement. This allows the relay platform to swing as the Kuroshio current direction changes. Typhoons occasionally pass through the mainstream of the Kuroshio. This issue can be addressed, for example, using a Spar platform, designed to operate continuously under storm conditions, to carry multiple current energy harvesters [44].

The design of a spar platform is analogous to that of naval architecture, with stability under varying wave conditions being a critical consideration [44]. Unlike vessels, spar platform design must also account for the weight of the mooring lines, which is influenced by water depth and dictates the required length of the mooring lines. To support all applied loads (both live and dead), the platform’s total volume must be sufficiently large, and this volume is inherently linked to the

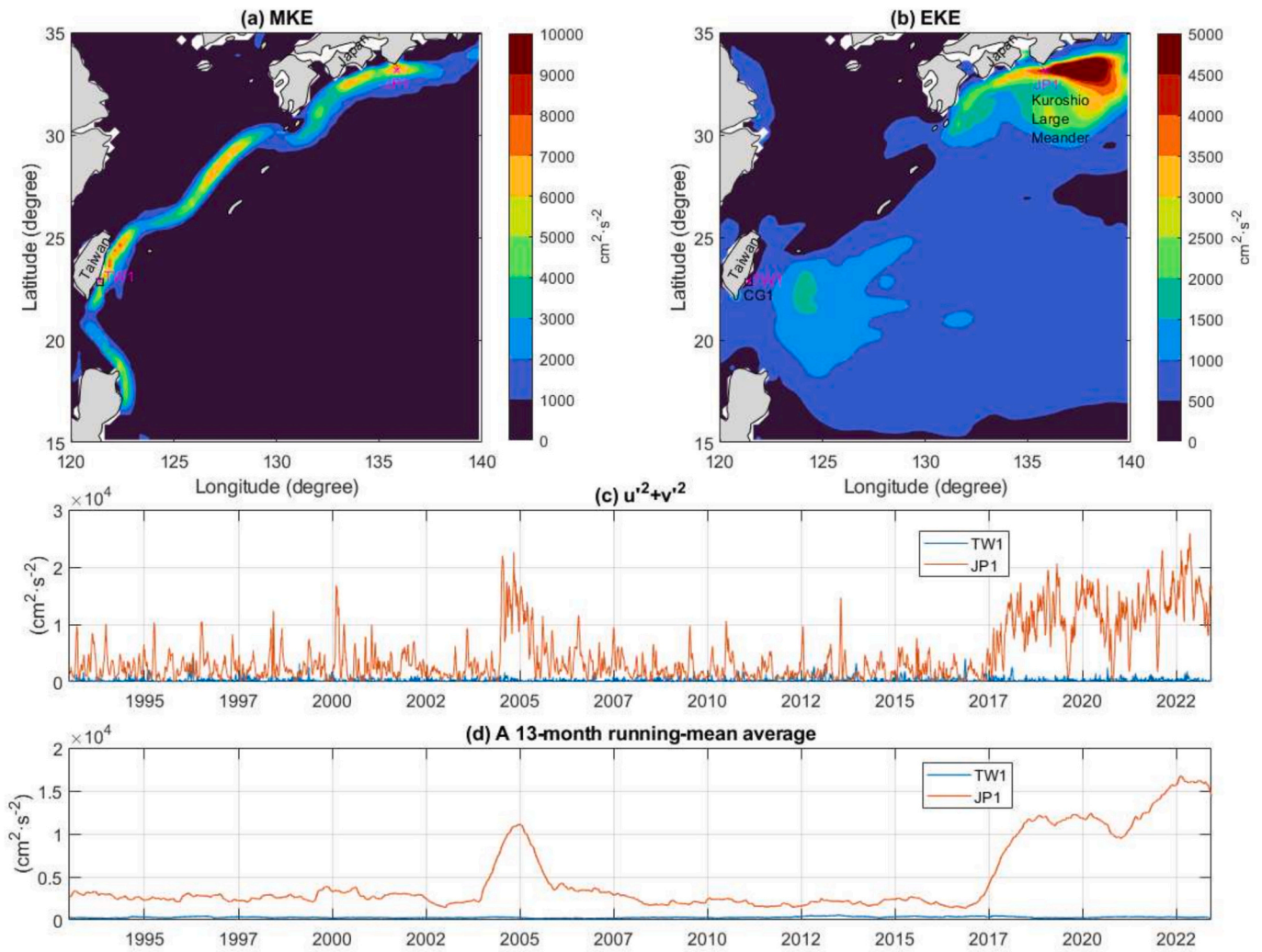


Fig. 12. Kinetic-energy structure and long-term variability of the Kuroshio Current derived from 31 years (1993–2023) of CMEMS altimeter-based surface velocities. (a) Mean kinetic energy (MKE, cm^2/s^2) highlighting the time-mean Kuroshio jet; the highest core values occur south of Japan and off eastern Taiwan. (b) Eddy kinetic energy (EKE) quantifies time-varying motions. EKE peaks in the Kuroshio-Large-Meander (LM) region south of Honshu, whereas variability is substantially lower east of Taiwan. Magenta markers denote the analysis points: TW1 (Taiwan shelf break) and JP1 (maximum-MKE grid cell south of Japan). (c) Monthly velocity variance ($u^2 + v^2$) at TW1 (blue) and JP1 (orange). (d) Time series of path-deflection after applying a 13-month centered running mean—the operational filter used by JMA to identify large-meander (LM) events, defined by path displacement persisting ≥ 1 yr. The smoothed JP1 record exceeds the LM threshold in 2005 and again from 2017 to present, corresponding to two documented LM episodes. In contrast, the TW1 series exhibits low variance with no LM signature, indicating a stable, shore-attached Kuroshio east of Taiwan. This quasi-steady behavior underpins the suitability of the TW1 (C1–C5) corridor for marine-current power generation. (For interpretation of the references to colour in this figure legend, the reader is referred to the web version of this article.)

platform's geometry. The geometry, in turn, directly impacts the platform's stability. These interdependencies between loads, volume, geometry, and stability highlight the complexity involved in designing an effective floating platform. Several companies and developers are producing larger current turbines for deep waters. The successful operation of the Kuroshio power plant in Japan or Taiwan will encourage the construction of other current power plants designed to access sustainable energy in suitable sites within other western boundary currents (Gulf Stream, Agulhas Current, etc.).

3.3. Underestimation of Kuroshio power

The theoretical available power (*TAP*) is defined as the maximum power available from the output power of a marine current turbine [14]. *TAP* is governed by the relationship described by Eq. (3):

$$TAP = \frac{1}{2} \rho A U^3 \quad (3)$$

where ρ (kg/m^3) is the seawater density; A (m^2) is the cross-sectional area of the turbine; and U (m/s) is the current velocity. In Japan, IHI built a 100 kW ($50 \text{ kW} \times 2$ units) current turbine with a rotor diameter of ~ 11 m and is planning to develop a large current turbine with a rated output of 2 MW ($1 \text{ MW} \times 2$ units) with a rotor diameter of ~ 40 m [17]. If the ocean current speed is 1 m/s, the *TAP* of one rotor is expected to increase from approximately 49 kW ($TAP = 0.5 \times 1028 \text{ kg}/\text{m}^3 \times 5.5 \text{ m} \times 5.5 \text{ m} \times 3.14 \times 1 \text{ m}/\text{s} \times 1 \text{ m}/\text{s} \times 1 \text{ m}/\text{s} = 48,822 \text{ W}$) to 646 kW ($TAP = 0.5 \times 1028 \text{ kg}/\text{m}^3 \times 20 \text{ m} \times 20 \text{ m} \times 3.14 \times 1 \text{ m}/\text{s} \times 1 \text{ m}/\text{s} \times 1 \text{ m}/\text{s} = 645,584 \text{ W}$) after upgrading from a 100 kW turbine to a 2 MW turbine.

For a typical current speed of 1.06 m/s at the C1 station, based on GDP data (Fig. 8) and a turbine rotor diameter of 40 m, the *TAP* is calculated to be approximately 769 kW ($TAP = 0.5 \times 1028 \text{ kg}/\text{m}^3 \times 20 \text{ m} \times 20 \text{ m} \times 3.14 \times 1.06 \text{ m}/\text{s} \times 1.06 \text{ m}/\text{s} \times 1.06 \text{ m}/\text{s} = 768,900 \text{ W}$). Conversely, for a typical speed of 0.77 m/s, according to the HYCOM+NCODA data at C1 (Fig. 11), and the same turbine rotor, the *TAP* is approximately 295 kW ($TAP = 0.5 \times 1028 \text{ kg}/\text{m}^3 \times 20 \text{ m} \times 20 \text{ m} \times 3.14 \times 0.77 \text{ m}/\text{s} \times 0.77 \text{ m}/\text{s} \times 0.77 \text{ m}/\text{s} = 294,730 \text{ W}$). This indicates

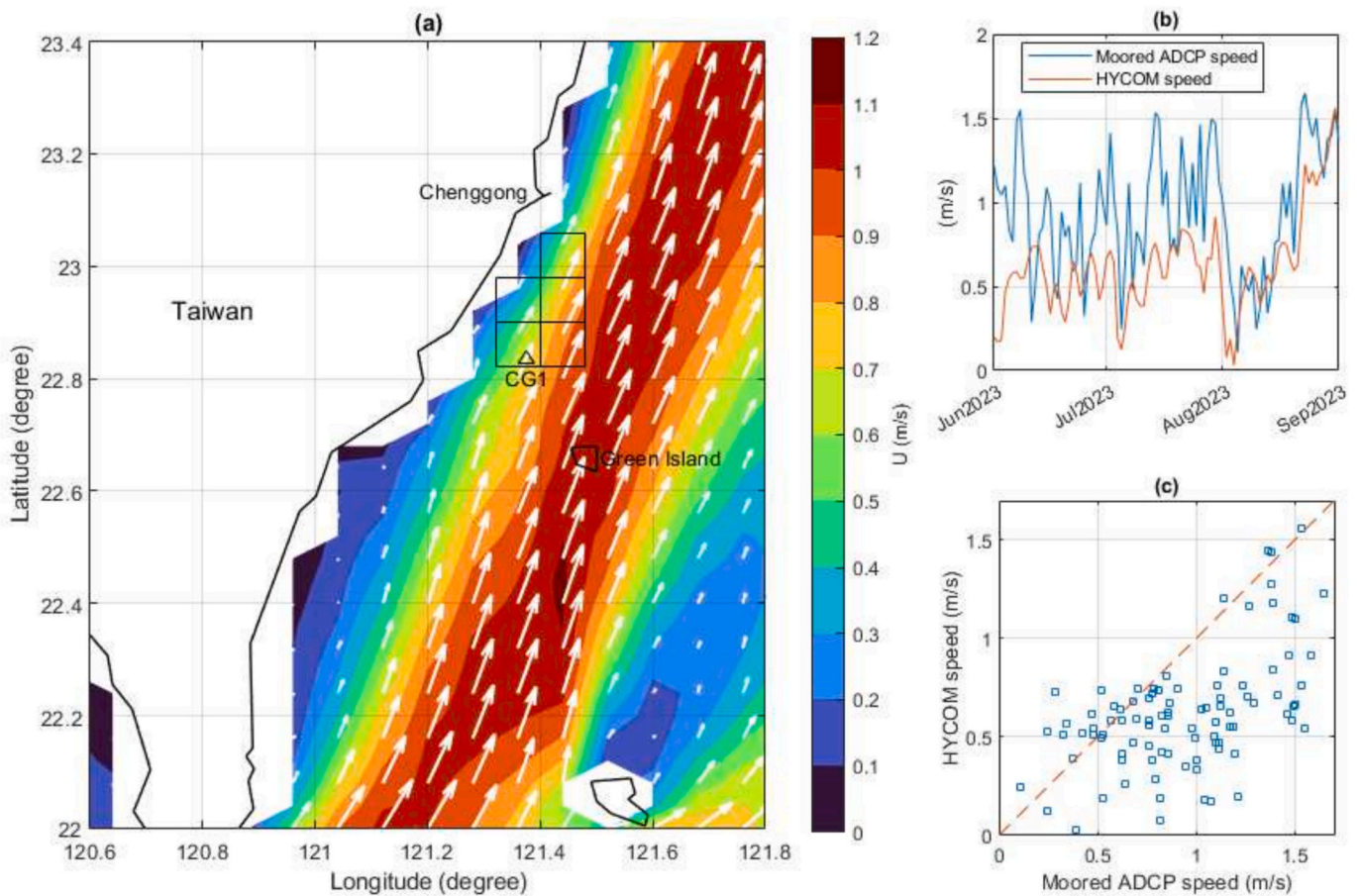


Fig. 13. Comparison of HYCOM+NCODA analysis against moored ADCP data for contemporary at site CG1 (40 m depth). (a) Mean current speed (m/s) and vectors derived from the HYCOM + NCODA 1/12° analysis for June–August 2023 off eastern Taiwan. The five highest-ranked candidate stations (C1–C5; black squares) and the CG1 ADCP location (black triangle) are indicated; Chenggong and Green Island are labelled for reference. (b) Time-series comparison of current speed at 40 m obtained from the moored ADCP (blue) and the HYCOM (orange) between 1 June and 1 September 2023. (c) Scatter plot of reanalysis speed versus observed speed; the dashed line marks the 1:1 relationship. The shallowest ADCP bin (40 m) recorded a mean speed of 0.94 ± 0.37 m/s, whereas the HYCOM + NCODA field at the same depth averaged 0.62 ± 0.29 m/s, underestimating the observed flow by $\sim 34\%$. We attribute this bias chiefly to the model's horizontal resolution (~ 8 km; cell area ~ 73 km²), which is too coarse to resolve Green Island (~ 15 km²). The unresolved island deflects the simulated Kuroshio core seaward, displacing the along-stream velocity maximum away from our near-shore sites C1–C5. (For interpretation of the references to colour in this figure legend, the reader is referred to the web version of this article.)

that the TAP is approximately 61 % lower when using the current speed from the HYCOM+NCODA model compared to the observational GDP current speed, suggesting that the HYCOM+NCODA model underestimates the Kuroshio current power by around 61 %.

Analyses by Qiu and Chen [45] reveal that, during the satellite-altimetry era beginning in 1993, the Kuroshio south of Honshu has entered a sustained Large-Meander (LM) regime on only two occasions, with transitions initiated in 2005 and again in 2017. We revisited this question with a 31-year (1993–2023) record of CMEMS satellite altimeter velocities (Fig. 12) and identified three key results. Maps of mean kinetic energy (MKE; Fig. 12a) and eddy kinetic energy (EKE; Fig. 12b) confirm that the time-mean jet is strongest off eastern Taiwan and south of Honshu, but time-varying energy is overwhelmingly concentrated in the Japanese LM corridor. The analysis points JP1 (maximum-MKE grid cell south of Japan) and TW1 (Taiwan shelf break, encompassing our candidate sites C1–C5) represent high-variance and low-variance end-members, respectively. Velocity variance at JP1 spikes in 2005 and 2017 (Fig. 12c). After applying the 13-month centered running mean used operationally by the Japan Meteorological Agency—thereby enforcing the ≥ 1 -yr persistence criterion—those two spikes remain the only intervals that exceed the long-term background (Fig. 12d), precisely reproducing the LM chronology reported by Qiu and Chen [45]. No comparable signal is present at TW1. The absence of any LM-scale path

displacement east of Taiwan over three decades indicates a quasi-steady, shore-attached Kuroshio jet. This stability reduces flow-resource intermittency and infrastructure-relocation risk, thereby reinforcing the techno-economic attractiveness of the TW1 (C1–C5) corridor for large-scale, sustainable ocean current energy development. Our independent satellite analysis confirms that the Taiwanese reach of the Kuroshio has remained dynamically stable since at least 1993—a favorable prerequisite for long-term renewable energy exploitation.

Accurate investment-grade design requires contemporaneous in situ measurements, such as bottom-mounted ADCPs, rather than sole reliance on coarse model data. Fig. 13 juxtaposes a three-month current record from the CG1 mooring with the co-located HYCOM+NCODA 1/12° field: at 40 m depth the ADCP registers 0.94 ± 0.37 m/s, whereas the model yields only 0.62 ± 0.29 m/s—a systematic shortfall of approximately 34 %. Given the cubic dependence of kinetic-power density on velocity, this bias amplifies to a $> 70\%$ error in the estimated resource. The root of the bias is primarily geometric: the HYCOM mesh (~ 8 km; ~ 73 km² per cell) cannot adequately resolve Green Island (~ 15 km²). The island's omission in the model deflects the simulated Kuroshio core seaward, away from the C1–C5 corridor. Three independent data sets, NOAA surface drifters, shipboard-ADCP sections, and the CG1 mooring—all capture the shore-attached branch that the model misses. When the shipboard transects are objectively analyzed on a 1/

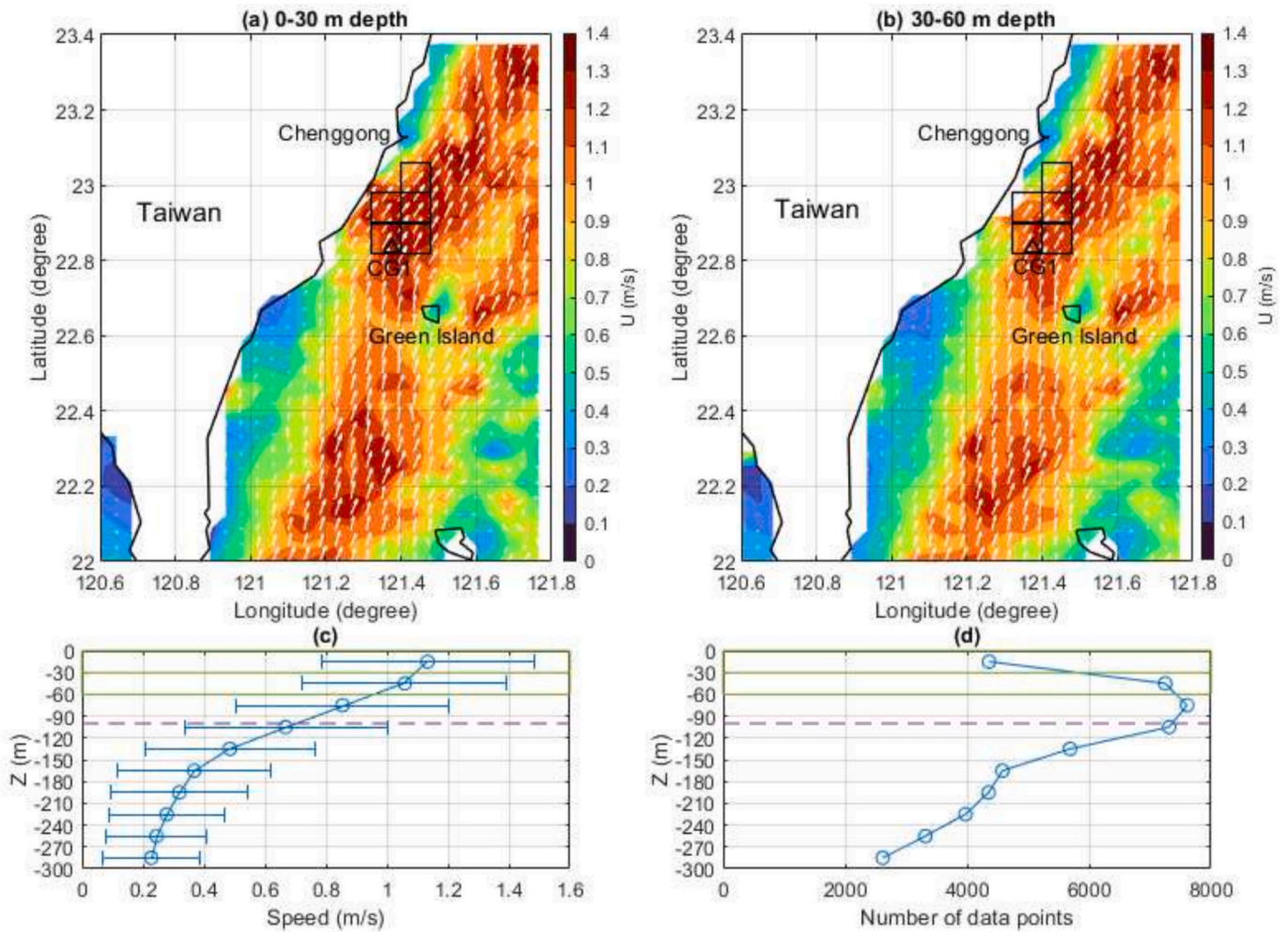


Fig. 14. High-resolution shipboard-ADCP view of the near-surface Kuroshio jet in the lee of Green Island and implications for turbine siting. (a) Mean current speed (m/s) and vectors in the 0–30 m layer, mapped on a $1/24^\circ$ grid (~ 4 km) from underway ADCP transects collected during June–September 2023. The five highest-ranking candidate stations C1–C5 (black squares) and the mooring site CG1 (black triangle) are shown; Chenggong and Green Island are labelled. (b) Same as (a) but for the 30–60 m layer. The high-resolution field clearly reveals the Kuroshio jet bifurcating around Green Island, with the stronger branch veering shore-ward and passing directly over C1–C5, a feature smeared out in the HYCOM + NCODA analysis. (c) Composite speed profile averaged over C1–C5 (blue circles) with one-standard-deviation bars. The green horizontal bar marks the nominal turbine-operating layer; the purple dashed line marks the storm-wave-protection depth (~ 100 m) to which the turbine is lowered during typhoons. Near-surface speeds average 1.10 ± 0.40 m/s, whereas the co-located HYCOM field at 15 m depth is 0.77 ± 0.17 m/s, indicating a $\sim 30\%$ underestimation. (d) Data-density histogram by depth confirms robust sampling of the upper 120 m. (For interpretation of the references to colour in this figure legend, the reader is referred to the web version of this article.)

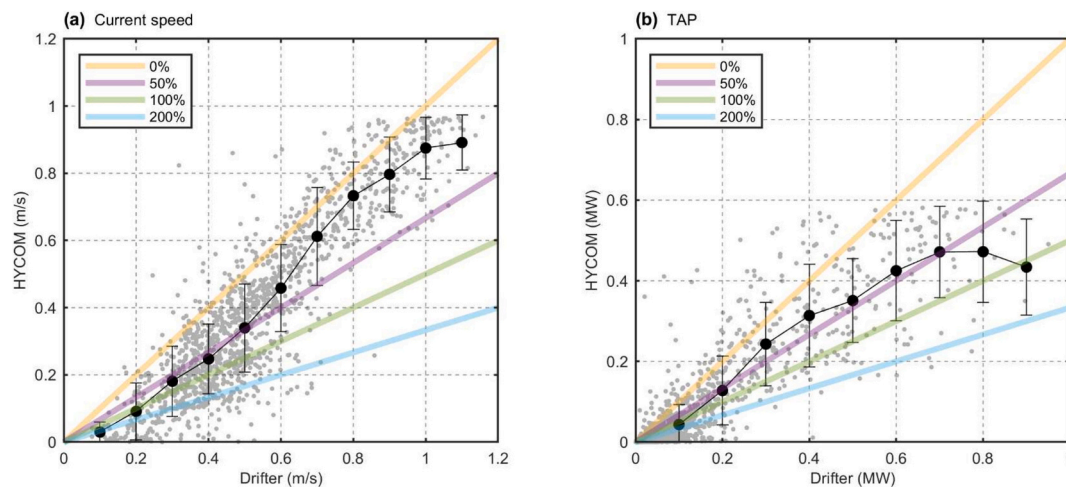


Fig. 15. (a) Current speeds based on GDP drifter data and HYCOM-NCODA reanalysis data (GLBu0.08). (b) TAP for a 2 MW current turbine based on GDP drifter data and HYCOM-NCODA model data. Oblique lines represent the percentage increase in drifter speed and TAP. Black dots represent the mean percentage increase in drifter speed and TAP with the error bars showing one standard deviation.

24° (~4 km) grid (Fig. 14), the jet is clearly seen to bifurcate around Green Island, with the stronger branch hugging the coastline and passing directly over sites C1–C5. In that 15 m layer, the shipboard field averages 1.10 ± 0.40 m/s, whereas HYCOM yields only 0.77 ± 0.17 m/s, representing a further approximate 30 % shortfall.

Taiwan's floating marine-current turbines are designed to maximize energy harvesting by continuously aligning with the velocity core of the Kuroshio Current. Vertical profiles collected from shipboard ADCPs across the C1–C5 corridor show that the peak flow occurs in the upper mixed layer, approximately 0–30 m below the surface (Fig. 14b). Assuming future maritime-exclusion zones maintain moderate restrictions, routine operating depths are expected to primarily range within the 30–50 m band. During typhoon events, the platforms can be ballasted down to approximately 100 m, positioning the rotor well beneath the storm-wave zone. This approach preserves structural integrity while still exploiting a substantial portion of the mean current energy.

Collectively, the evidence demonstrates that contemporary, site-specific moorings and high-resolution shipboard surveys are indispensable for Kuroshio Current energy projects. These methodologies ground-truth numerical model products, reveal sub-kilometer current steering mechanisms, and provide the confidence levels required by investors, insurers, and regulators. While regional reanalysis models remain valuable as preliminary screening tools, only in situ measurements—capable of resolving features on the scale of Green Island—can reduce risk in Kuroshio projects to bankable standards and enable reliable turbine-array optimization.

Since, in the past, power generation was estimated based on the current speed simulated using a numerical model, the power generation capacity of Kuroshio and even that of the Gulf Stream have been significantly underestimated. Fig. 15 illustrates the 15 m-depth current velocities and the corresponding available power (TAP) for a 2 MW turbine with a 40 m rotor diameter, computed from GDP drifter observations and HYCOM + NCODA model outputs. In the Kuroshio mainstream ($U=0.7\text{--}1.1$ m/s in Fig. 4), the TAP is increased by 50–100 %, as depicted in Fig. 15, when GDP drifter data are compared with HYCOM+NCODA data. In the anticipated region, the power generation increases by approximately 83 % ($(859,270 \text{ W} - 470,630 \text{ W})/470,630 \text{ W} = 0.8258$) while the drifter speed is 1.1 m/s ($TAP = 0.5 \times 1028 \text{ kg/m}^3 \times 20 \text{ m} \times 20 \text{ m} \times 3.14 \times 1.1 \text{ m/s} \times 1.1 \text{ m/s} \times 1.1 \text{ m/s} = 859,270 \text{ W}$) and the model speed is 0.9 m/s ($TAP = 0.5 \times 1028 \text{ kg/m}^3 \times 20 \text{ m} \times 20 \text{ m} \times 3.14 \times 0.9 \text{ m/s} \times 0.9 \text{ m/s} \times 0.9 \text{ m/s} = 470,630 \text{ W}$). All three independent in situ data sources—NOAA Global Drifter trajectories, high-

resolution shipboard ADCP transects, and the CG1 moored ADCP record—consistently show near-surface mean speeds that are 25–35 % higher than those in the collocated HYCOM + NCODA data. Due to the cubic relationship between velocity and kinetic power density, this discrepancy translates into a systematic underestimation of approximately 70 % in the model-derived energy resource assessment for the southeastern Taiwan Kuroshio corridor.

4. Conclusion

1. Higher Kuroshio Energy Potential: Previous estimations of power generation potential often relied on model-simulated current speeds, which tend to underestimate the energy available. Observational data reveals that the kinetic power density in the Kuroshio mainstream is approximately 70 % higher than model-based estimates, highlighting a significantly greater sustainable energy potential.
2. Site Determination: Six suitable sites within the Kuroshio were identified using GDP drifter data. Among these, the five most suitable sites (C1–C5), spanning an area of approximately 365 km², have the potential to accommodate 1150 turbines, collectively generating about 0.7 GW of power. Beyond the Kuroshio, additional potential exists in regions such as the Gulf Stream. Promising locations include offshore areas near Miami and West Palm Beach, Florida, where favorable conditions support Gulf Stream power generation (see Fig. 16). These findings underline the vast global potential for ocean current power as a sustainable energy resource.
3. Stable Kuroshio Jet Off Taiwan: Thirty-one years of CMEMS altimetry data confirm only two sustained Large-Meander events—occurring 2005 and 2017—which were confined to the Japanese Kuroshio corridor identified by Qiu and Chen [45]. In contrast, the branch east of Taiwan exhibits persistently low variance with no meanders, maintaining a shore-attached, quasi-steady jet. This dynamical stability minimizes resource intermittency and eliminates relocation risk, thereby establishing the TW1/C1–C5 sector as a bankable, utility-scale marine current energy prospect. These characteristics strengthen Taiwan's renewable energy portfolio and enhance its future energy mix.
4. Capacity Factor of Ocean Current Turbines and Future Work: This study established the relationship between current (or towing) speeds and CF, providing a foundation for estimating energy production and LCOE at potential sites. For current speeds of 0.5, 0.7, 0.9, 1.1, 1.3, and 1.5 m/s, the corresponding CF values are 0, 0.08, 0.19, 0.34, 0.52, and 1.00, respectively. A 30 MW pre-commercial

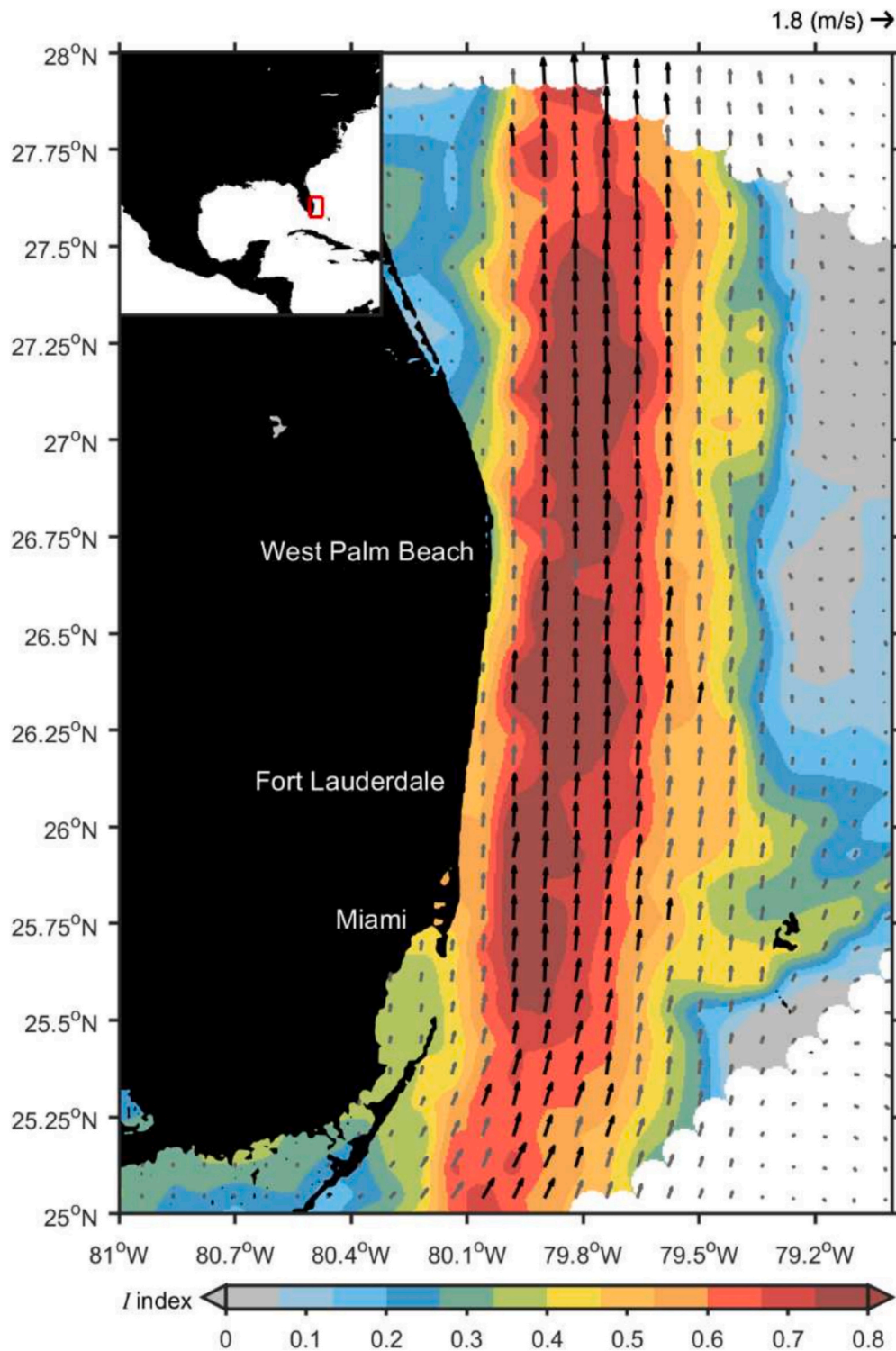


Fig. 16. Distribution of the feasibility index (I) in the Gulf Stream region. Averaged drifter velocities (arrows) in $1/12^\circ \times 1/12^\circ$ bins. Speeds higher and lower than 1.2 m/s are shown in black and gray, respectively.

Kuroshio array would require a present-value capital investment of approximately US \$146 million, resulting in seasonal LCOE values of US \$94–113 per MWh in summer and US \$187–283 per MWh in winter. These cost variations reflect seasonal differences in depth-averaged current velocities: 1.2–1.3 m/s (capacity factor ~ 0.50 – 0.60) in summer versus 0.9–1.0 m/s (capacity factor ~ 0.20 – 0.30) in winter at the optimal deployment site. Scaling the array to 100 MW is projected to reduce the LCOE by approximately

50 %, with independent analyses [40] indicating potential values approaching US \$54 per MWh under mature deployment conditions.

CRediT authorship contribution statement

Yu-Chia Chang: Writing – original draft, Validation, Methodology, Conceptualization. **Chau-Ron Wu:** Writing – review & editing, Supervision, Conceptualization. **Peter C. Chu:** Writing – review & editing.

You-Lin Wang: Writing – review & editing, Visualization. **Luca R. Centurioni:** Data curation. **Guan-Yu Chen:** Supervision, Software. **Ruo-Shan Tseng:** Data curation.

Funding sources

This research did not receive any specific grant from funding agencies in the public, commercial, or not-for-profit sectors.

Declaration of competing interest

The authors declare that they have no known competing financial interests or personal relationships that could have appeared to influence the work reported in this paper.

Acknowledgements

The authors would like to acknowledge the Grants from the Academia Sinica. Peter C. Chu was supported by the U.S. DoD Strategic Environment Research and Development Program (SERDP). We are grateful for the comments of editor and reviewers.

Data availability

Data will be made available on request.

References

- [1] UN General Assembly, Transforming our world: the 2030 Agenda for Sustainable Development. <https://www.refworld.org/docid/57b6e3e44.html>; 2023. Accessed 11 August.
- [2] Bajah AS. Generating electricity from the oceans. *Renew Sust Energ Rev* 2011;15:3399–416.
- [3] Owusu PA, Asumadu-Sarkodie S. A review of renewable energy sources, sustainability issues and climate change mitigation. *Cogent Engineering* 2016;3(1):1167990.
- [4] Shadman M, Roldan-Carvajal M, Pierart FG, Haim PA, Alonso R, Silva C, et al. A review of offshore renewable energy in South America: current status and future perspectives. *Sustainability* 2023;15(2):1740.
- [5] Hernández-Fontes JV, Felix A, Mendoza E, Cueto YR, Silva R. On the marine energy resources of Mexico. *J Mar Sci Eng* 2019;7(6):191.
- [6] Meyer I, Van Niekerk JL. Towards a practical resource assessment of the extractable energy in the Agulhas Ocean current. *Int J of Mar Energy* 2016;16:116–32.
- [7] Hanson HP, Skemp SH, Alsenas GM, Coley CE. Power from the Florida current: a new perspective on an old vision. *Bull Am Meteorol Soc* 2010;91:861–6.
- [8] Duerr AES, Dhanak M. An assessment of the hydrokinetic energy resource of the Florida current. *IEEE J Ocean Eng* 2012;37:281–93.
- [9] Hanson HP. Gulf stream energy resources: North Atlantic flow volume increases create more power. *Ocean Eng* 2014;87:78–83.
- [10] Kabir A, Lemongo-Tchamba I, Fernandez A. An assessment of available ocean current hydrokinetic energy near the North Carolina shore. *Renew Energy* 2015;80:301–7.
- [11] Chen F. Kuroshio power plant development plan. *Renew Sust Energ Rev* 2010;14:2655–68.
- [12] Hsu TW, Liau JM, Liang SJ, Tzang SY, Doong DJ. Assessment of Kuroshio current power test site of Green Island, Taiwan. *Renew Energy* 2015;81:853–63.
- [13] Chen F, Lu SM, Tseng KT, Lee SC, Wanga E. Assessment of renewable energy reserves in Taiwan. *Renew Sust Energ Rev* 2010;14:2511–28.
- [14] Barnier B, Domina A, Gulev S, Molines JM, Maître T. Modelling the impact of flow-driven turbine power plants on great wind-driven ocean currents and the assessment of their energy potential. *Nat Energy* 2020;5(3):240–9.
- [15] VanZwieten JH, Meyer I, Alsenas GM. Evaluation of HYCOM as a tool for ocean current energy assessment, proceedings of the 2nd marine energy technology symposium, METS14. 2014.
- [16] Shirasawa K, Tokunaga K, Iwashita H, Shintake T. Experimental verification of a floating ocean-current turbine with a single rotor for use in Kuroshio currents, *renew. Energy* 2016:189–95.
- [17] Corporation IHI. IHI demonstrated the world's Largest Ocean current turbine for the first time in the world. *IHI Engr Rev* 2019;52(1):6–9.
- [18] Wanchi Steel Ltd. <http://www.wanchi.com.tw/Default.aspx?lang=en-US>; 2023. Accessed 5 July.
- [19] Chen YY, Hsu HC, Bai CY, Yang Y, Lee CC, Cheng HK, et al. Evaluation of Test Platform in the Open Sea and Mounting Test of KW Kuroshio Power-Generating Pilot Facilities. In: Proceedings of the 2016 Taiwan Wind Energy Conference. Taiwan: Taipei; 2016. p. 24–6 [in Chinese].
- [20] Yeh PH, Tsai SY, Chen WR, Wu SN, Hsieh MC, Chen BF. A simple nozzle-diffuser duct used as a Kuroshio energy harvester. *Processes* 2021;9:1552. <https://doi.org/10.3390/pr9091552>.
- [21] NOAA. Database Update Status. <https://www.aoml.noaa.gov/phod/gdp/index.php>; 2023. Accessed 5 July.
- [22] Ocean Data Bank, Shipboard ADCP data. <https://www.odb.ntu.edu.tw/en/>; 2025. Accessed 2 May.
- [23] CMEMS. Global Ocean Gridded L 4 Sea Surface Heights And Derived Variables Reprocessed. Ongoing; 1993. https://data.marine.copernicus.eu/product/SEA_LEVEL_GLO_PHY_L4_MY_008_047/description. Accessed 2 May 2025.
- [24] HYCOM + NCODA Global 1/12° Reanalysis/Analysis. <https://www.hycm.org/dataserver/gofs-3pt0/reanalysis>; 2025. Accessed 2 May.
- [25] Niiler PP, Sybrandy AS, Bi K, Poulain PM, Bitterman D. Measurements of the water following capability of holey-sock and TRISTAR drifters. *Deep-Sea Res* 1995;42A:1951–64.
- [26] NOAA, Six-Hourly Interpolated Data. <https://www.aoml.noaa.gov/phod/gdp/int/erpolated/data/all.php>; 2023. Accessed 5 July.
- [27] Cummings JA. Operational multivariate ocean data assimilation. *Quart J Royal Met Soc, Part C* 2005;131(613):3583–604.
- [28] Cummings JA, Smedstad OM. Variational data assimilation for the Global Ocean. *Data Assimilation for Atmospheric, Oceanic and Hydrologic Applications* 2013;13:303–43.
- [29] Chang YC, Tseng RS, Chu PC. Site selection of ocean current power generation from drifter measurements. *Renew Energy* 2015;80:737–45.
- [30] Tseng RS, Chang YC, Chu PC. Use of global satellite altimeter and drifter data for ocean current resource characterization, marine renewable energy. *Resource Characterization and Physical Effect* 2017:159–77.
- [31] Freeland HJ. Statistical observations of the trajectory of neutrally buoyant floats in the North Atlantic. *J Mar Res* 1975;33:383–404.
- [32] Centurioni LR, Niiler PP. On the surface currents of the Caribbean Sea. *Geophys Res Lett* 2003;30:1279. <https://doi.org/10.1029/2002GL016231>.
- [33] Centurioni LR, Niiler PP, Lee DK. Observations of inflow of Philippine Sea surface water into the South China Sea through the Luzon Strait. *J Phys Oceanogr* 2004;34:113–21.
- [34] Lee DK, Niiler PP. The energetic surface circulation patterns of the Japan. *East Sea, Deep-Sea Res* 2005;52(II):1547–63.
- [35] Chang YC, Chen GY, Tseng RS, Centurioni LR, Chu PC. Observed near-surface flows under all tropical cyclone intensity levels using drifters in the northwestern Pacific. *J Geophys Res* 2013;118:2367–77.
- [36] Wang G, Wu L, Mei W. Ocean currents show global intensification of weak tropical cyclones. *Nature* 2022;611:496–500.
- [37] Wang F, Zhang L, Feng J, et al. Atypical seasonal variability of the Kuroshio current affected by intraseasonal signals at its origin based on direct mooring observations. *Sci Rep* 2022;12:13126.
- [38] Taiwan Power Company, Electricity purchased and sold in. <https://dmz26.moea.gov.tw/GA/common/Common.aspx?code=M&no=2>; 2023. in Chinese. Accessed 26 June 2024.
- [39] Taiwan Power Company, The Energy Bureau's 2024 annual carbon emission coefficient. <https://www.taipower.com.tw/2764/2826/2842/2845/25145/normPost>; 2025. Accessed 2 May.
- [40] Minesto. Minesto's technology transforms ocean energy into one of the most cost-effective energy resources, new Cost of Energy analysis states. 2017. p. 2017. <https://minesto.com/news/minestos-technology-transforms-ocean-energy-into-one-of-the-most-cost-effective-energy-resources-new-cost-of-energy-analysis-states/>.
- [41] Chen F. *The Kuroshio power plant*. 1 ed. Springer International Publishing; 2013. p. 320.
- [42] TETHYS. MeyGen Tidal Energy Project. <https://tethys.pnnl.gov/project-sites/meygen-tidal-energy-project-phase-i>; 2023. Accessed 4 July.
- [43] Finkl CW, Charlier R. Electrical power generation from ocean currents in the straits of Florida: some environmental considerations. *Renew Sust Energ Rev* 2009;13:2597e604.
- [44] Yeh PH, Tsai SY, Chen WR, Hsu SM, Chen BF. A platform for Kuroshio energy harvesters. *Ocean Eng* 2021;223:108693. <https://doi.org/10.1016/j.oceaneng.2021.108693>.
- [45] Qiu B, Chen S. Revisit of the occurrence of the Kuroshio large meander south of Japan. *J Phys Oceanogr* 2021;51:3679–94.